universität
wien

DIPLOMARBEIT

Titel der Diplomarbeit

The role of Langerhans cells in skin cancer growth and immune response to Imiquimod

angestrebter akademischer Grad

Magister/Magistra der Naturwissenschaften (Mag. rer.nat.)

Verfasserin / Verfasser:	Nicole Amberg
Studienrichtung /Studienzweig (lt. Studienblatt):	Molekulare Biologie A490
Betreuerin / Betreuer:	Prof. Dr. Maria Sibilia,
	Prof. Dr. Marcela Hermann

Wien, am 27.09.2010

Durchgeführt an der Medizinischen Universität Wien, Institut für Krebsforschung, Innere Medizin I, Abteilung molekulare und zelluläre Tumorbiologie unter der Leitung von Univ. Prof. Dr. Maria Sibilia.

Acknowledgements

Abstract

Dendritic cells are the main antigen processing and presenting cells in the body. One subset of dendritic cells is the Langerhans cells (LCs), which are localized in the epidermis. Under steady-state conditions they continuously migrate to skin-draining lymph nodes and present antigen to naïve T cells. Under inflammatory conditions, LC migration is enhanced and their cytokine release is increased, activating and recruiting other types of immune cells to the site of inflammation. It has been shown in our lab that Imiquimod, a Toll-like receptor (TLR)7 agonist, activates LC and can lead to the regression of skin tumours like melanoma. In human therapy it is successfully used in treatment of basal-cell carcinoma (BCC). However, the role of LC in mediation of the antitumor effect of Imiquimod is poorly understood. In my thesis I addressed the question, if the presence of LCs has any impact on skin tumour growth and if they are important mediators of the antitumor effect of Imiquimod.

To address this question I employed two different mouse skin cancer models: (1) a syngeneic melanoma model, whereby B16F10 melanoma cells are injected intradermally into *LangerinDTR:EGFP* mice; and (2) mice carrying the SmoothenedM2 transgene (*Rosa26SmoM2YFP* mice) that can be induced to develop BCC.

(1) LCs were not responsible for the antitumoral effect of Imiquimod in the B16F10 melanoma model. Tumour bearing mice treated with Imiquimod showed decreased tumour growth rates compared to untreated control mice. This result was obtained independent of presence of LCs. Analysis of the cellular composition of tumour infiltrates revealed a role of LCs in recruiting CD8+ T cells and MHCII$^+$CD4$^+$ cells to Imiquimod-treated tumours as well as a regulatory role on mast cell degranulation.

(2) *Rosa26SmoM2YFP* mice were crossed to *K5Cre^{ERT}* and *LangerinDTR:EGFP* mice to give rise to inducible BCC bearing mice which can be depleted of LCs (*SmoM2LangerinDTR* mice). Imiquimod application onto BCC for 2 weeks did not have any influence on tumour growth. Therefore experiments using extended treatment regimens are planned.

Zusammenfassung

Dendritische Zellen sind die wichtigsten antigenprozessierenden und – präsentierenden Zellen des Körpers. Die Langerhanszellen stellen eine Subpopulationen von dendritischen Zellen dar. Sie sind in der Epidermis lokalisiert und nehmen unter physiologischen Bedingungen beständig Antigen auf, migrieren zu hautdränierenden Lymphknoten und präsentieren Antigen an naive T Zellen. Während Entzündungsprozessen wird die Langerhanszell-Migration erhöht, ebenso ihre Freisetzung von Zytokinen. Dadurch werden andere Immunzell-Populationen aktiviert und zur Entzündungsstelle rekrutiert. Eine Studie in unserem Labor konnte zeigen, dass Imiquimod, ein Toll-like Rezeptor (TLR)7 Agonist, Langerhanszellen aktiviert und darüber hinaus zur Regression von Hauttumoren, wie z.B. Melanomen, führt. In humaner Therapie wird Imiquimod häufig in der erfolgreichen Behandlung von Basaliomen eingesetzt. Dennoch ist bisher nicht bekannt, welchen Beitrag die Langerhanszellen zur Wirkweise des antitumoralen Effekts von Imiquimod leisten. In meiner Diplomarbeit habe ich die Fragestellung bearbeitet, ob die Präsenz von Langerhanszellen einen Einfluss auf das Wachstum von Hautkrebs hat und ob sie wichtige Übermittler des antitumoralen Effekts von Imiquimod darstellen.

Aus diesem Grund habe ich für die Studie zwei verschiedene Mausmodelle für Hautkrebs verwendet: (1) ein syngenes Melanom-Modell, wobei B16F10 Melanomzellen intradermal in *LangerinDTR:EGFP* Mäuse injiziert werden; und (2) Mäuse, bei welchen das Wachstum von Basaliomen durch Expression eines hyperaktiven Smoothened-Allels induziert werden kann (*Rosa26SmoM2YFP* Mäuse).

(1) Langerhanszellen sind nicht für den antitumoralen Effekt von Imiquimod im B16F10 Melanom-Modell verantwortlich. Tumore, die mit Imiquimod behandelt werden, weisen langsamere Tumorwachstumsraten auf als unbehandelte Tumore. Dieses Resultat kann unabhängig von der Präsenz von Langerhanszellen beobachtet werden. Die Analyse der zellulären Zusammensetzung von Tumorinfiltraten zeigt, dass Langerhanszellen eine Rolle in der Rekrutierung von CD8$^+$ T Zellen und MHCII$^+$CD4$^+$ Zellen in Imiquimod-behandelte Tumore spielen. Ebenso scheinen Langerhanszellen

einen regulatorischen Einfluss auf die Degranulation von Mastzellen auszuüben.

(2) *Rosa26SmoM2YFP* Mäuse wurden mit *K5-CreERT* und *LangerinDTR:EGFP* Mäusen gekreuzt, um einen Experimentenstamm (*SmoM2LangerinDTR* Mäuse) zu erhalten, in dem Basaliome induziert und Langerhanszellen depletiert werden können. Daher sind weitere Experimente über längere Behandlungszeiträume geplant.

TABLE OF CONTENT

1. <u>Introduction</u>

1.1 The skin

The skin is the largest organ of the vertebrate body, made up of multiple layers of tissue of ectodermal origin. The functions of the skin are various: it serves as a barrier to the surrounding environment, anatomically and immunologically protecting the body from pathogen entrance (Tomic-Canic 1998). It also serves as a somatosensory system via its different nerve endings. Furthermore, the skin plays a major role in body heat regulation, evaporation, water resistance, respiration, and synthesis and storage of lipids and water (Proksch 2008).

Skin layers of mammals are referred to as epidermis, dermis and subcutis (Eckert 1989) (figure 1). The human epidermis consists of five different layers: (1) stratum basale, (2) stratum spinosum, (3) stratum granulosum, (4) stratum ludicum, and (5) stratum corneum. On their way from basal layer to stratum corneum cells undergo morphological and biochemical changes, characterizing the transitional cell layers of the epidermis (Tomic-Canic 1998; Freedberg 2001). The major cell type of the epidermis is the keratinocyte (Nestle 2009), constituting more than 90% of the epidermis.

In the stratum basale the stem cells of the epidermis reside. Cells of this layer are undifferentiated and possess the ability to proliferate. During asymmetrical cell divisions, daughter cells migrate outwards and differentiate along this route to replenish the stratum corneum. Terminal differentiation gives rise to fully keratinized cells. The stratum spinosum contains keratinocytes which still contain their nucleus, but already start to keratinize. Additionally, desmosomal junctions lead to the characteristical appearance of this epidermal layer, functioning as anatomical water barrier. In the stratum granulosum, keratinocytes are called granular cells, since they contain high amounts of keratohyalin and lamellar granules. Keratohyalin helps in cell dehydration for cell flattening and in aggregation and cross-linking keratin fibers for keratinization. Keratinocytes of the overlaying stratum ludicum are already flattened and dead. The outermost epidermal layer, the stratum corneum, is composed of dead cells lacking nuclei, which are highly keratinized, achieving an efficient prevention of water evaporation.

Keratinocytes are known to have immunomodulatory function by either secretion of inhibitory cytokines like Interleukin (IL)-4 and transforming growth factor (TGF)β

(Freedberg 2001), or release of pro-inflammatory cytokines like tumor necrosis factor (TNF)α or IL-1β (Tomic-Canic 1998; Freedberg 2001). The latter are capable of activating another cell type of the epidermis, the Langerhans cells. Other cells homing in the epidermis are Merkel cells, melanocytes and epidermal T cells.
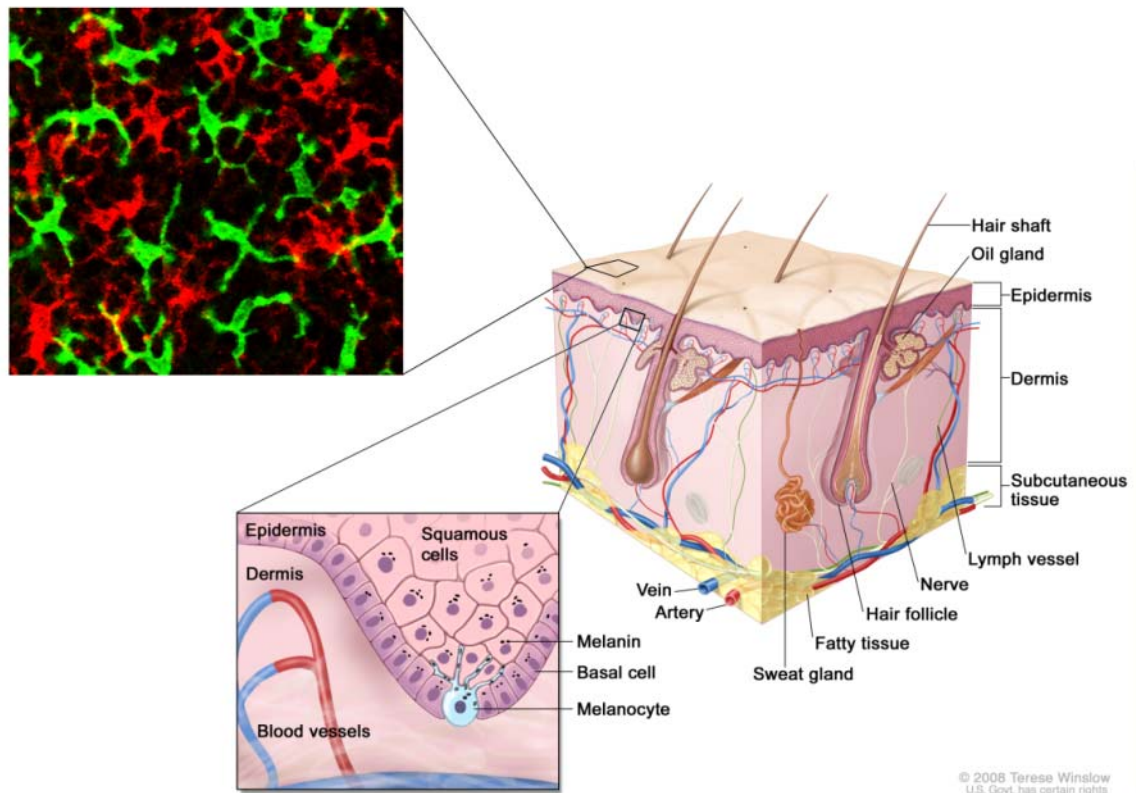
Fig. 1: scheme of skin morphology (adapted from Terese Winslow, National Institute of Cancer, Visuals Online) & network of epidermal immune cells (Langerhans cells and γδ T cells red: MHC-II; green: CD3ε; murine epidermis from the ear of a C57BL/6 mouse.

Melanocytes, which are the pigment producing cells of the skin, are primarily resident in the basal cell layer in humans, whereas in mice they are mainly located in dermal regions surrounding the hair follicle (Bosenberg 2003).

In mice, the skin resident T cell population expresses the alternative γδ T cell receptor (TCR), therefore called γδ T cells (Boismenu and Havran 1998; Laird 2009; Raulet 1989; Tigelaar 1990). They exhibit dendritic shape and, like Langerhans cells, form a network within the epidermis (figure 1). Their function remains unclear, but they are thought to be involved in innate immunity and wound healing (Toulon 2009).

1.2 Dendritic cells

Dendritic cells (DCs) function as professional antigen-presenting cells (APCs) and are found in all tissues that are in close contact to the environment (intestine, lung, skin) (Naik 2007). They serve in antigen uptake, processing and presentation to T cells in lymph nodes (Cisse 2008). In mammals, two main divisions of DCs exist: myeloid DCs (mDCs) and plasmacytoid DCs (pDCs) (Asselin-Paturel and Trinchierl 2005; Barchet 2005; Cao and Liu 2007). All murine DCs express the common surface marker molecule Cluster of Differentiation (CD)11c. The mDCs can be further divided into several subpopulations, characterized by expression of different surface molecules like CD4, CD8, CD11b or F4/80 (Shortman 2002).

In mice, CD4$^+$ DCs are the most prominent DC subtype in the spleen, and display only a minor fraction of lymph node DCs. CD4 is not only found on mDCs, but also known to be expressed on pDCs. CD8$^+$ DCs are present in the spleen, as well as in skin-draining and mesenteric lymph nodes, but most prominent in the thymus. These cells are the only known DC subtype that does not express CD11b on its surface. Recent studies observed, that CD8$^+$ DCs have the ability to induce a T helper 1 (T$_H$1)-biased cytokine response in reactive CD4$^+$ T cells and produce valuable amounts of IL-12p70, whereas CD8$^-$DCs tend to induce a T helper 2 (T$_H$2)-biased response (Maldonado-López 1999, Moser 2000). The CD8 molecule is also expressed in low levels on LCs. Another molecule that is found on LCs is the F4/80 surface marker, which is also present on macrophages and is thought to play in role in immunological tolerance (van den Berg 2005).

1.2.1 Langerhans cells

LCs are found in the epidermis, where they form a continuous network to take up foreign antigens via their extended dendrites (Merad 2008; Schuler 1993; Valladeau 2005). It is believed that besides circulating haematopoietic precursor cells, a skin homing LC progenitor exists, which could not be identified so far (Gilliam 1998; Holt 1994; Merad 2002). Although, several studies could show, that LCs repopulate locally independently of bone-marrow-derived progenitors in the steady state (Merad

2002). During inflammatory conditions, LCs derived from blood circulating monocytic precursors can also reconstitute the population (Merad 2004).

Langerin (CD207) is a type II C-type lectin receptor that serves as a valuable marker for LCs in humans and mice and is involved in the uptake of pathogens (Valladeau 2000). After internalization, Langerin is found in newly formed organelles called Birbeck granules, which are thought to function in antigen-processing (Birbeck 1961; Mc Dermott 2002; Wolff 1967). Other characterizing surface molecules of LCs are major histocompatibility complex (MHC) class II (MHC-II), CD11c, CD11b, E-Cadherin, epidermal cell adhesion molecule (EpCAM), and F4/80 (Borkowski 1996; Stingl 1980; Tang 1993). In humans, LCs additionally express CD1a at high levels (Romani 2006). E-Cadherin serves as an epidermal anchorage protein that links LCs to the neighbouring keratinocytes. After antigen uptake LCs emigrate to skin-draining lymph nodes (sDLN) and present antigen to naive T cells (Stoitzner 2006). In migratory LCs, which constantly emigrate to LNs in the steady state, E-Cadherin is strongly downregulated, whereas CD11c, CD11b, EpCAM, and F4/80 expression remains stable (Jakob 2001). In contrast, MHC class II (MHC-II) as well as co-stimulatory and migratory molecules like CD40 and C-C chemokine receptor (CCR)7 are strongly upregulated (Karjalainen 2000; Ohl 2004; Pierre 1997). During inflammatory conditions, migration rate of LCs increases (Hemmi 2001; Macatonia 1987; Stoitzner 2005). Migratory LCs can be found in the sDLN ~4 days after antigen-uptake in the epidermis (Kissenpfennig 2005).

There are other dendritic cell subtypes present in the skin, referred to as dermal dendritic cells (dDCs) and further subdivided into Langerin[+] and Langerin[-] dDCs. They do not only differ in expression of Langerin, but also in the presence of surface molecules CD11b, CD103, and F4/80 (Poulin 2007). Together, three different dDC subsets can be identified: Langerin^{-}CD11b^{+}, Langerin^{+}CD11b^{low} and Langerin^{-}CD11b^{low} expressing DCs (Shklovskaya 2008). These dDCs show different migratory behavior than LCs, since after antigen uptake the migration of Langerin^{-}CD11b^{+} and Langerin^{+}CD11b^{low} dDCs peaks after 1 day, whereas that of Langerin^{-}CD11b^{low} dDCs peaks at 2 days (Kissenpfennig 2005; Shklovskaya 2008). DDCs function in antigen presentation and chemokine secretion to initiate proinflammatory responses (Nestle 2009). A scheme of skin APCs and their surface markers is depicted in figure 2.
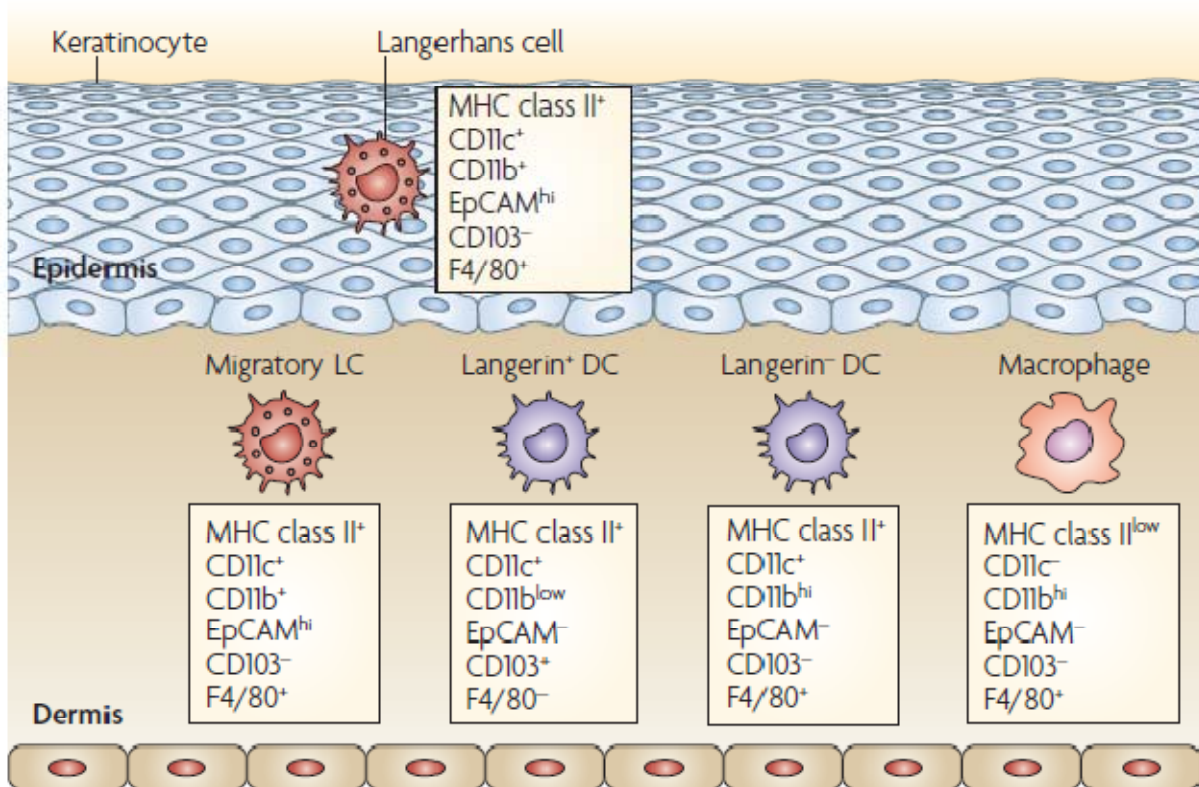
Fig. 2: schematic picture of skin immune cells of monocytic origin and their surface markers (from Merad, 2008).

So far, controversial opinions exist among the scientific community about the immunological function of LCs. Dependent on experimental setup and immunological environment they may exhibit immunogenic or tolerogenic function. *In vitro* studies show that LCs isolated from human skin are capable of cross-presenting antigen to $CD8^+$ T cells, as well as to induce a T_H1 response (Klechenvsky 2008). Additional studies show that in contact-hypersensitivity response (CHS) LCs are required for cutaneous sensitization to haptens when antigen is administered to the epidermis (Stoitzner 2008). On the other hand, several studies suggest a role for LCs in tolerance: LCs induced deletional tolerance of self-reactive $CD8^+$ T cells in a transgenic mouse model, in which keratinocytes expressed membrane-bound ovalbumin (Waithman 2007). Another study – using transgenic mice overexpressing CD40Ligand by keratinocytes – shows, that LCs activated *in situ* may break tolerance to tissue antigens, leading to systemic autoimmune disease (Mehling 2001).

1.2.2 Plasmacytoid dendritic cells

The function of pDCs diverges from that of mDCs, since upon stimulation and activation pDCs produce large amounts of type I interferons, mainly interferon α (IFNα) (Cao 2009). Type I interferons are employed to stimulate macrophages and natural killer (NK) cells to elicit an antiviral immune response, as well as mDCs, B and T cells (Colonna 2004; Gilliet 2008; Piqueras 2006; Jego 2003; Le Bon 2003; Kolumam 2005). Characteristically, pDCs exhibit plasma-cell morphology and coexpress marker molecules B220, CD4, CD11c, GR-1, and MHC-II (Palamara 2004). In mice, resting pDCs predominantly express Toll-like receptor (TLR) 7 and TLR9, both functioning in detection of nucleic acids in endosomal cell compartments (Cisse; Jarosay 2001). TLR7 can be stimulated by ssRNA molecules (Diebold 2001) and by members of a family of small molecules, the imidazoquinolines, to which the compounds Imiquimod and Resiquimod belong (Heil 2004; Jurk 2002). TLR9 recognizes ssDNA molecules containing unmethylated CpG motifs (Hemmi 2000). Both TLRs are associated with the signal transduction protein MyD88, which serves as an adaptor molecule to transduce the signal via assembly of a protein complex composed of tumor necrosis factor (TNF) receptor associated factor (TRAF)6, Bruton´s tyrosine kinase (BTK), and interleukin-1-receptor-associated kinase (IRAK)4 (Gilliet 2008). Further downstream, this results in gene expression of proinflammatory cytokines IFNα, IFNβ, IFNλ, IFNω, IL-6, TNF, and costimulatory activation molecules CD40, CD80, and CD86 (figure 3) (Gilliet 2008; Kadowaki 2001).
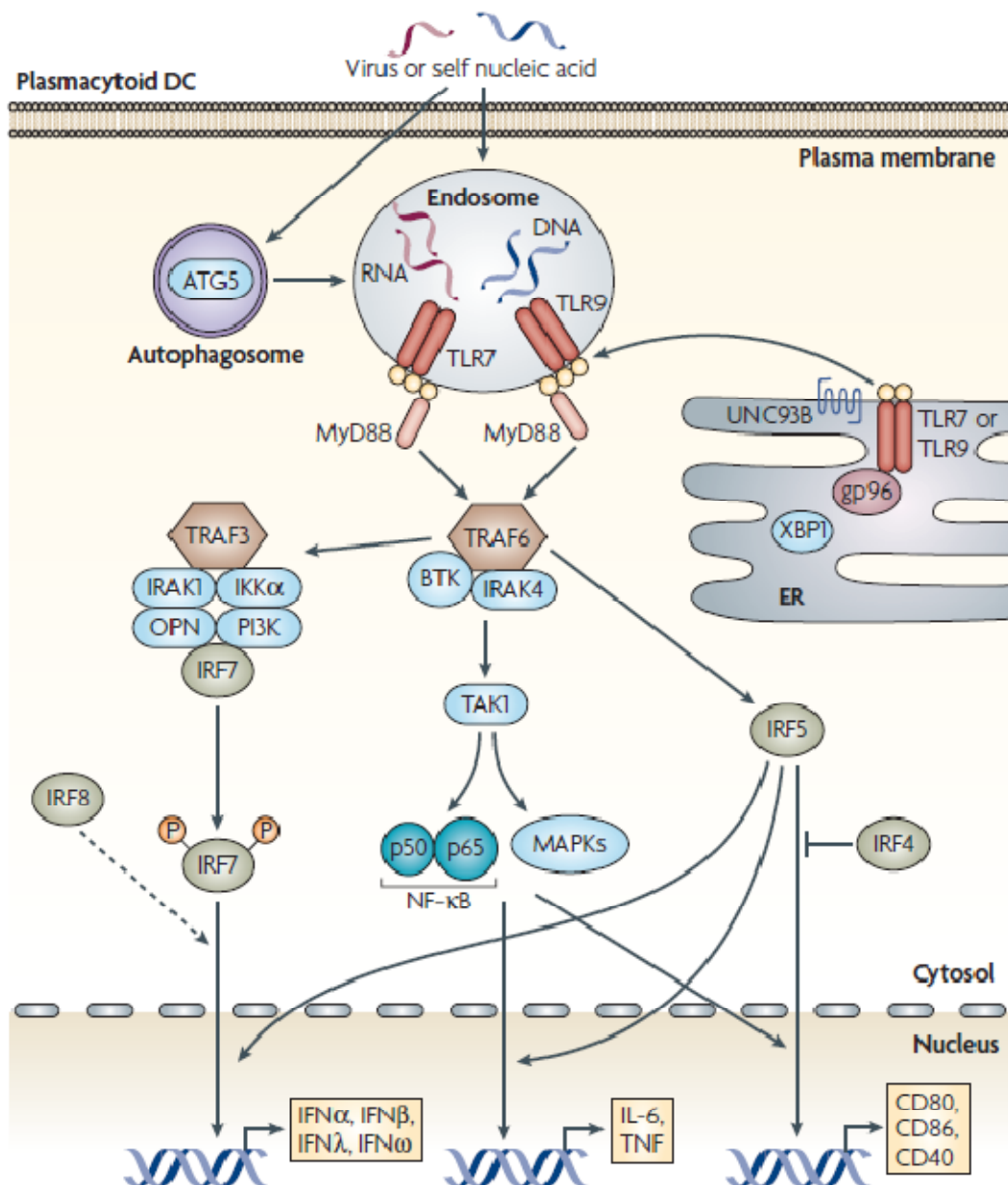
Fig. 3: scheme of TLR7 or TLR9 induced activation of pDCs and TLR-downstream signaling (from Gilliet, 2008)

1.3 Skin cancer

Skin cancers are the most common malignancies in the white population. More than 3.5 million skin cancers are diagnosed annually in the United States of America (Rogers 2010.). There are 2 main types of skin cancers: (1) melanoma and (2) non-

melanoma skin cancer, which themselves are further subdivided into basal-cell carcinoma and squamous-cell carcinoma.

1.3.1 Melanoma

Melanoma accounts for only a small portion of all skin cancers, but is the type with the highest mortality since it exhibits a highly aggressive behavior and preferentially metastasizes to liver, lungs and brain. The etiology of melanoma is believed to arise from DNA damage caused by UV irradiation (Maddodi 2008), starting with a benign nevus that includes aberrantly proliferating melanocytes (Miller 2006). These hyperprofliferating cells lead to the formation of a hyperplastic lesion, which by overcoming senescence enters the next step in melanoma development: dysplasia (Gray-Schoper 2006; Mooi 2006). A dysplastic nevus can enter the radial growth phase (RGP), which is defined by superficial spreading, confinement to epidermis and low invasive potential. When cells gain the ability to invade the dermis, this stage is referred to as vertical growth phase (VGP) and is characterized by metastasis (figure 4) (Miller 2006).
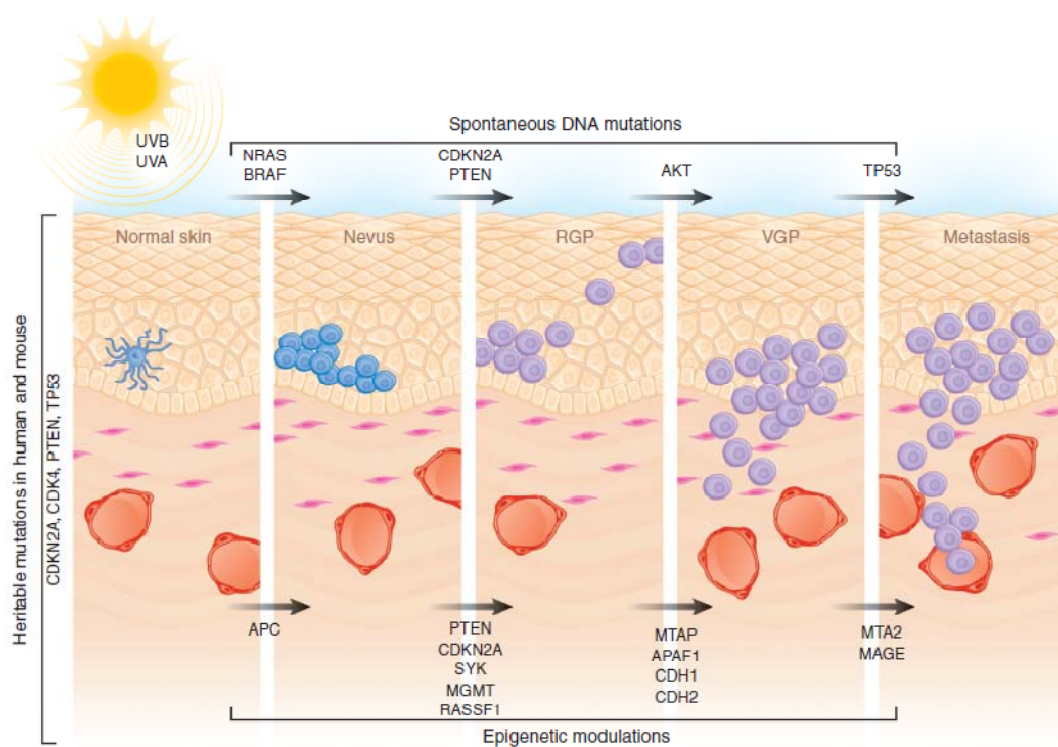
Fig. 4: scheme of the stepwise formation of melanoma, also showing characteristical genes to be mutated in this type of skin cancer (from Zaidi, 2008)

1.3.2 Basal-cell carcinoma

Basal-cell carcinoma (BCC) is the most common type of skin cancer with an incidence of 30% of Caucasian developing BCC during their life (Epstein 2008; Gaitanis 2009). BCC is a rarely metastasizing type of non-melanoma skin cancer but still considered to be malignant. The appearance of BCC is a slow-growing, translucent, elevated lesion accompanied by telangiectasia and in most cases pigmentation (Rubin 2002). BCC can be subcategorized into three major groups: superficial BCC, nodular BCC and the aggressive infiltrative BCC. A molecular signaling pathway that is affected in a high percentage of BCCs is the Hedgehog (Hh) pathway (Gailani 1996; Xie 1998). In mammals there exist three different extracellular Hh ligands: sonic hedgehog (SHH), indian hedgehog (IHH), and desert hedgehog (DHH). All variants of Hh bind to the membrane receptor patched (PTCH1), which upon Hh binding releases its inhibitory function on another membrane protein called Smoothened (SMO). Once this inhibition is suppressed and SMO is recruited to the site of Hh interaction, it sends activating signals to suppressor of fused (SUFU) and further downstream to the members of the GLI transcription factor family: GLI1, GLI2, and GLI3 (Lum 2004). Since the Hh pathway interacts with other growth factor signaling pathways (EGFR, PDGFRα), and activates the PI3K-Akt, MAPK and Wnt pathways, it integrates many proliferative signaling cascades (Schnidar 2009; Xie 2001). UV irradiation is a major cause of DNA damage in the basal layer of the epidermis (Kricker 1995), leading to CT -> T and CC -> TT transitions, which are also referred to as "UVB signature mutations" (Lund and Timmins 2007). Mutations on human chromosome 9q22, where the PTCH1 gene is located, are known to be present in patients suffering from basal-cell nevus syndrome (or Gorlins syndrome) (Gailani 1992; Johnson 1996). These mutations are giving rise to a loss-of-function of the inhibitory activity of the PTCH1 protein on the Hh pathway. Other Hh pathway affecting mutations were found in the smoothened (SMO) gene, an oncogene which, after point mutation, can acquire constitutive activity and lead to an active Hh signalling, thereby driving cell proliferation (figure 5) (Reifenberger 2005). Since UV-exposure also leads to damage and emigration of LCs from the epidermis and abnormal antigen-presentation of skin antigens, this inducible depression of the local immune system of the skin may depress immunosurveillance for tumor cells and additionally lead to DNA damage favoring skin cancer development (Granstein, 2004).
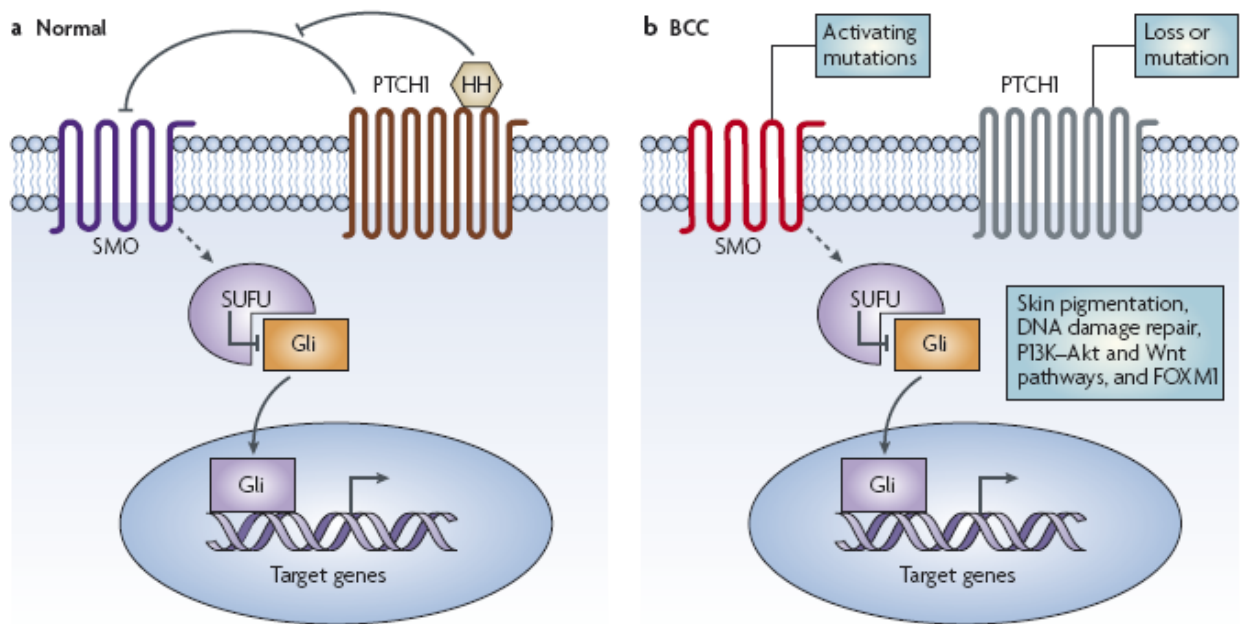
Fig. 5: scheme of normal (A, left) and aberrant (B, right) Hedgehog signaling (from Epstein, 2008)

1.3.3 Squamous cell carcinoma

Squamous-cell carcinoma (SCC) is a malignant tumour of the squamous epithelium of the epidermis. Like BCC it usually occurs in body regions which are exposed to sun light and is therefore thought to be caused by UV irradiation induced DNA damage. Also immunosuppression might be a risk factor for SCC. The metastasizing potential is low, but higher than for BCC (Clark 2008; Huang 2009). As previously shown by our lab, SCC survival is strongly dependent on EGFR signaling as well as on autocrine VEGFR signaling (Fig.6, Sibilia 2010). In a transgenic mouse model expressing a hyperactive form of the Ras activator Son of Sevenless (Sos) from the keratin5 promoter (*K5-SOS* mice), these mice develop spontaneous skin papillomas. K5-SOS activates expression of VEGFR, e.g. Flt1, and its ligands, resembling a situation similar to human SCC where overexpression of Flt1 can be observed (Bergers and Benjamin 2003, Ferrara 2003).
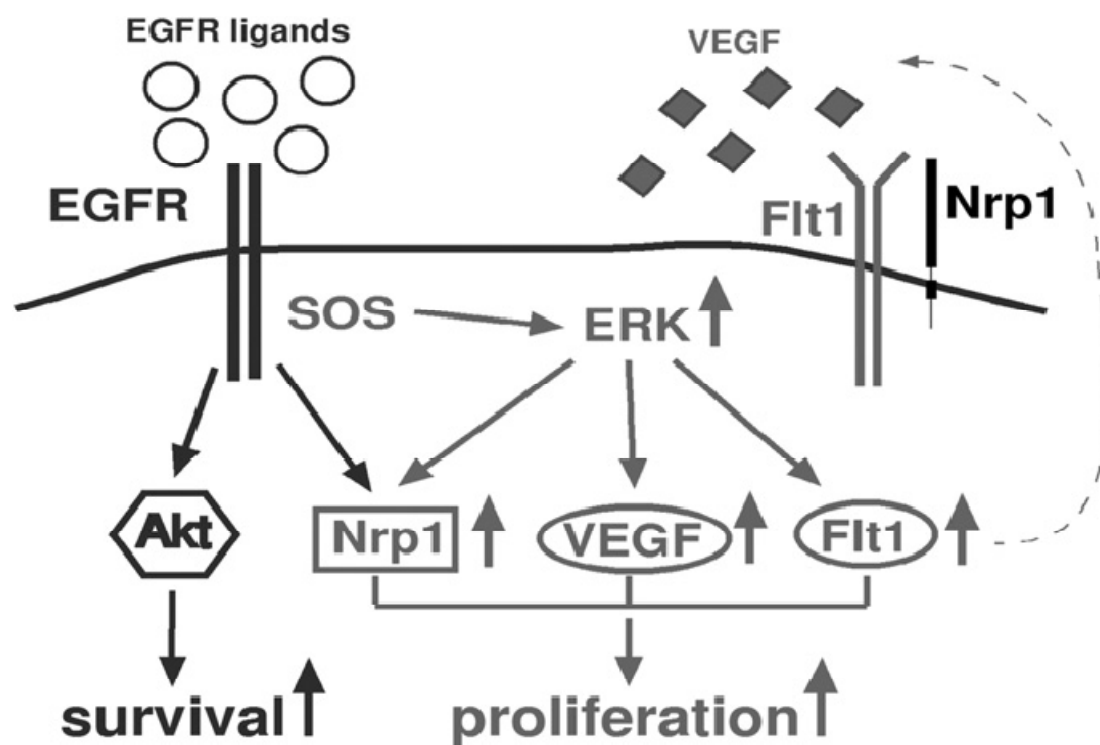
Fig. 6 Autocrine VEGF synergizes with EGFR in tumor cells to promote epithelial cancer development (Lichtenberger 2010).

1.4.4 Skin cancer therapies

Treatment of skin cancers includes (1) surgery, (2) cryotherapy, (3) photodynamic therapy, (4) chemotherapy and/or (5) immunotherapy, which may also be used in different combinations. For low-risk disease, chemo-, immuno- and cryotherapy are carried out to control the progression of the tumour. (1) Surgical techniques are subdivided into Moh´s micrographic surgery, simple or shave excision, electrodesiccation, laser surgery, dermabrasion, and cryosurgery. The most commonly used surgical method in skin cancer therapy is Moh´s excision, where the tumor is cut from the skin in thin layers. During surgery, the edges of the tumor and each layer of tumor removed are viewed through a microscope to check for cancer cells and to remove as little healthy tissue as possible. (2) Cryotherapy employs an instrument to freeze and destroy abnormal tissue. (3) For photodynamic therapy (PDT) a drug that is not active until it is exposed to light is injected into a vein. The drug collects more in cancer cells than in normal cells. When laser light is shined onto the skin the drug becomes active and cancer cells die. (4) Chemotherapeutical agents are commonly taken orally and lead to cancer cell death or inhibit their

proliferation. In case of skin cancer, these drugs are often applied topically to the tumor. (5) Immunotherapy involves topical treatment of cancer with Resiquimod or Imiquimod, thereby activating the immune system of the patient to induce tumor clearance.

The compound Imiquimod is contained at a concentration of 5% in the cream Aldara and acts as an immune response modifier by binding to Toll-like receptor (TLR) 7 and the adenosin receptor A_{2A} to activate signaling cascades of the innate immune system. TLR7 activation leads to release of pro-inflammatory cytokines like Interleukin (IL) 6, interferon (IFN) α, and tumor-necrosis factor (TNF) α (Hemmi 2002). A T_H1 response is initiated, recruiting CD8^{+} T cells with effector function to the site of Imiquimod application, thereby reducing the tumor volume (Huang 2009; Nakajima 2001). Recent studies showed that Imiquimod application leads to the activation and reversible emigration of LCs (De Giorgi 2009, Palamara 2004, Suzuki 2000). The immune cell infiltrate was shown to not only consist of CD8^{+} T cells, but also of additional cell types like natural killer (NK) cells, pDCs, macrophages and B-cells (Miller 1999; Palamara 2004). There are more studies showing that Imiquimod exerts its antitumoural function independently of immunomodulation by either upregulating opioid growth factor receptor (OGFR) expression (Zagon 2008), leading to inhibition of cell proliferation, or via upregulation of Bax (Schön 2004), promoting enhanced tumour cell apoptosis.

1.5 Mouse skin cancer models
There exist different models to study melanoma initiation and progression: (1) UVR-induced melanoma (Noonan 2001); (2) graftment of human melanoma onto immunocomprimised mice (Berking 2004); (3) murine melanoma derived from autochthonous murine or genetically engineered mouse (GEM) tumors transplanted into immunocompetent syngeneic mice (Fidler and Kripke 1977); (4) GEM melanoma with similar history to human disease (Ackermann 2005; Chin 2006; Gupta 2005); and (5) graftment of murine melanoma to GEM hosts (Yu 2002) (figure 6).
Animal models for BCC include mice with deficiency in PTCH1 (Corcoran 2001; Hahn 1997) or activating mutations in SMO (Mao 2006), leading to a constitutively active Hh signaling pathway, thereby driving cell proliferation.
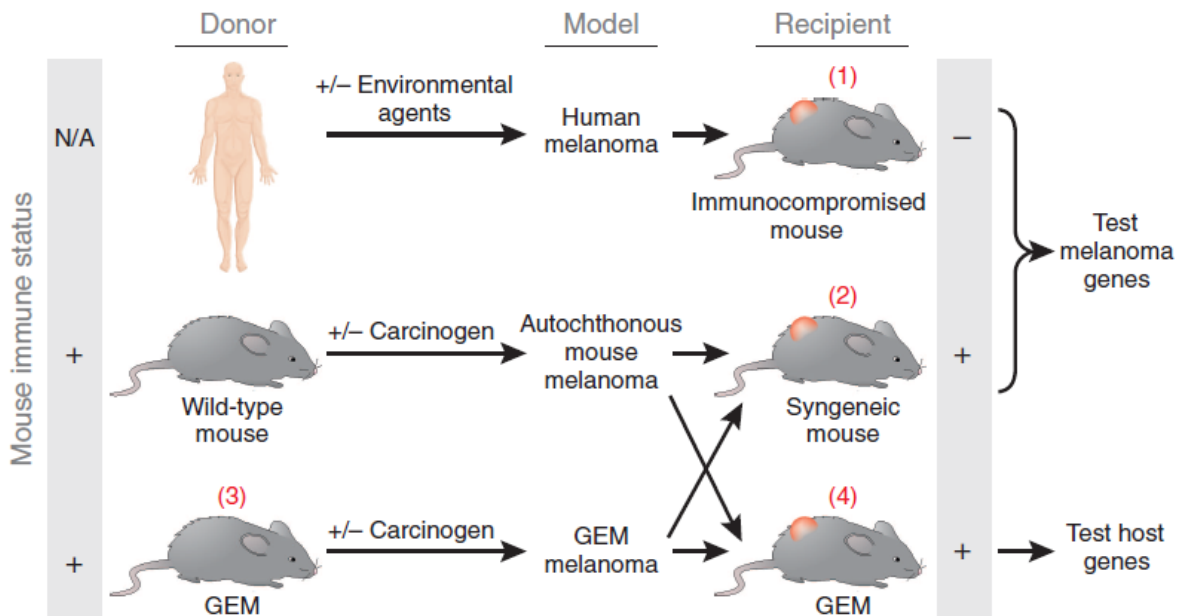
Fig 7.: different mouse models for melanoma studies (from Zaidi, 2008)

1.6 Mouse models used

Two different mouse model systems were chosen: (1) to study whether Imiquimod is still therapeutically active in the absence of LCs after intradermal injection of B16F10 melanoma cells into syngeneic *LangerinDTR:EGFP* mice; and (2) to study the role of LCs in BCC treatment, mice harboring a constitutively active form of the *smo* gene, SmoM2, were treated with Imiquimod. As this study requires mice with an intact immune system without any compromission and also a normal stroma, both mouse models were of C57BL/6 background.

(1) The B16 murine melanoma and its individual sublines were generated by Fidler and Kripke in 1977. B16F10 melanoma cells were intradermally injected into *LangerinDTR:EGFP* mice, which harbor a transgene consisting of the sequence of the human diphteria toxin (DT) receptor (DTR) fused to the sequence of enhanced green fluorescent protein (EGFP) under the control of the murine langerin promoter (figure 7). When DT is injected intraperitonially (i.p.) to mice, DT will be able to enter all cells, which express the DTR and induce their apoptosis. DTR expression thereby enables uptake of i.p. applied DT to deplete Langerhans cells from murine skin. A limitation of this system is

given by the fact, that not only the LCs are depleted of the skin, but also the langerin-expressing dDCs.
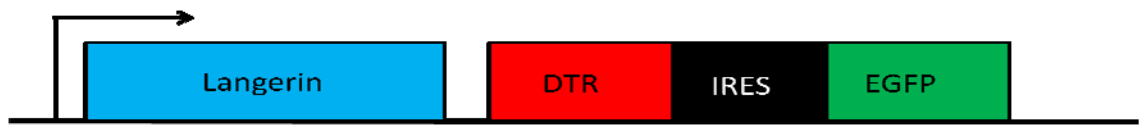
Fig. 8: scheme of the *LangerinDTR:EGFP* transgene

(2) The BCC model employs Smoothened transgenic mice, harboring a constitutively active form of the *smo* gene, called SmoM2, under the control of the ubiquitously expressed Rosa26 locus. In front of the *smoM2* gene a Neomycin stop-cassette is inserted, which is flanked by LoxP sites. These mice were crossed in the C57BL/6 background to mice harboring a Keratin5 (K5) Cre^{ERT} (K5-Cre^{ERT}) transgene. K5 is mainly expressed in the basal layer of the skin. By injecting tamoxifen to these mice, Cre recombinase can translocate to the nucleus and remove the floxed stop-cassete. Thereby expression of the hyperactive *smo* gene is induced, resulting in development of skin alterations similar to BCC in these mice.

R26SmoM2:YFP mice were also crossed to *LangerinDTR:EGFP* mice to allow development and progression of BCC in WT and LC depleted mice.
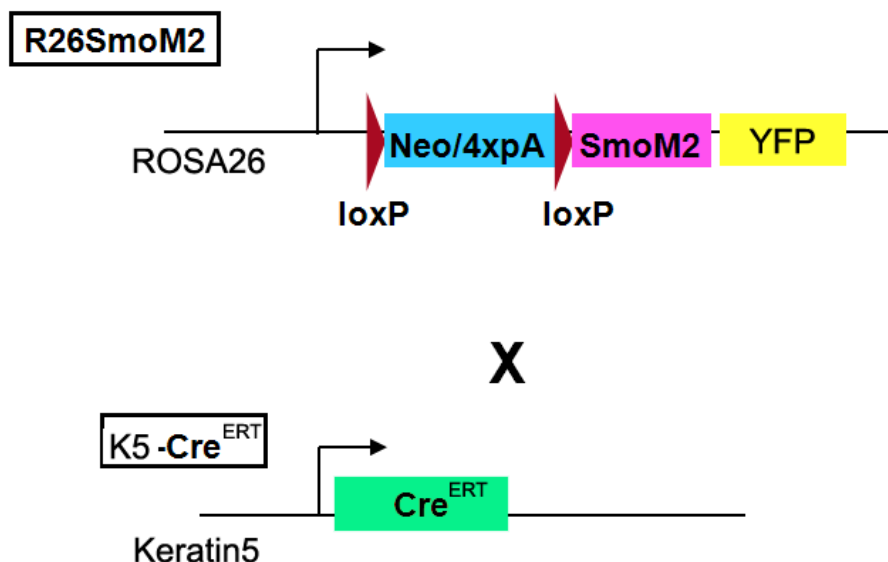
Fig. 9: breeding scheme of mice harboring the *R26SmoM2:YFP* transgene and mice harboring the *K5-Cre^{ERT}* transgene.

2. **Aim of thesis**

Since Langerhans cells (LCs) exert a profound role in skin immunology, my study adressed the question, which impact LCs have on skin cancer growth and if they are necessary for Imiquimod´s action as an anti cancer drug. As recent studies confirmed an activation of LCs upon Imiquimod treatment and enhanced infiltration of pDC-like cells to the site of topical Imiquimod application (Palamara 2004), there might be a correlation between both events.

To answer, whether there is a correlation of LC-presence and tumor growth during Imiquimod treatment, *LangerinDTR:EGFP* mice were subcutaneously injected with B16F10 melanoma cells. Tumor growth was monitored in WT mice and mice depleted of LCs, as well as in Imiquimod treated WT and LC-depleted mice to observe possible effects of LC on tumor progression. Tumors were examined histologically for infiltrating immune cells, especially pDC-like cells and T cells, since these cell populations are thought to play a major role in antitumoral immune activity.

During my study, I established a second mouse model system of skin cancer in the lab: *R26SmoM2:YFP* mice were crossed to K5-Cre[ERT] transgenic mice to allow development and progression of basal-cell carcinoma (Ref). To further be able to study the role of LCs in this model, these mice were crossed to *LangerinDTR:EGFP* mice. After development of BCC lesions, mice were treated with Imiquimod to reveal its antitumoral activity in this model. Tumor growth and characterization of skin morphological changes were monitored histologically. The distribution of epidermal immune cell was analyzed by immunofluorescence staining on frozen sections.

3. Results

3.1 Effect of Imiquimod on WT murine skin

To evaluate the ability of Imiquimod to activate LCs not only in humans (De Giorgi 2009), but also in mice, ears of C57BL/6 wilde-type (WT) mice were creamed with Aldara for seven consecutive days and analyzed by histology and FACS. Immunofluorescence staining of epidermal ear sheets for langerin revealed an activated morphology of LCs: cells had less dendrites, contained a larger cell body and an increased staining intensity for MHC-II was observed (figure 10). The total number of LCs in the Imiquimod-treated ears decreased compared to non-treated ears, confirming an emigration of activated LCs from the epidermis (Palamara, 2004).
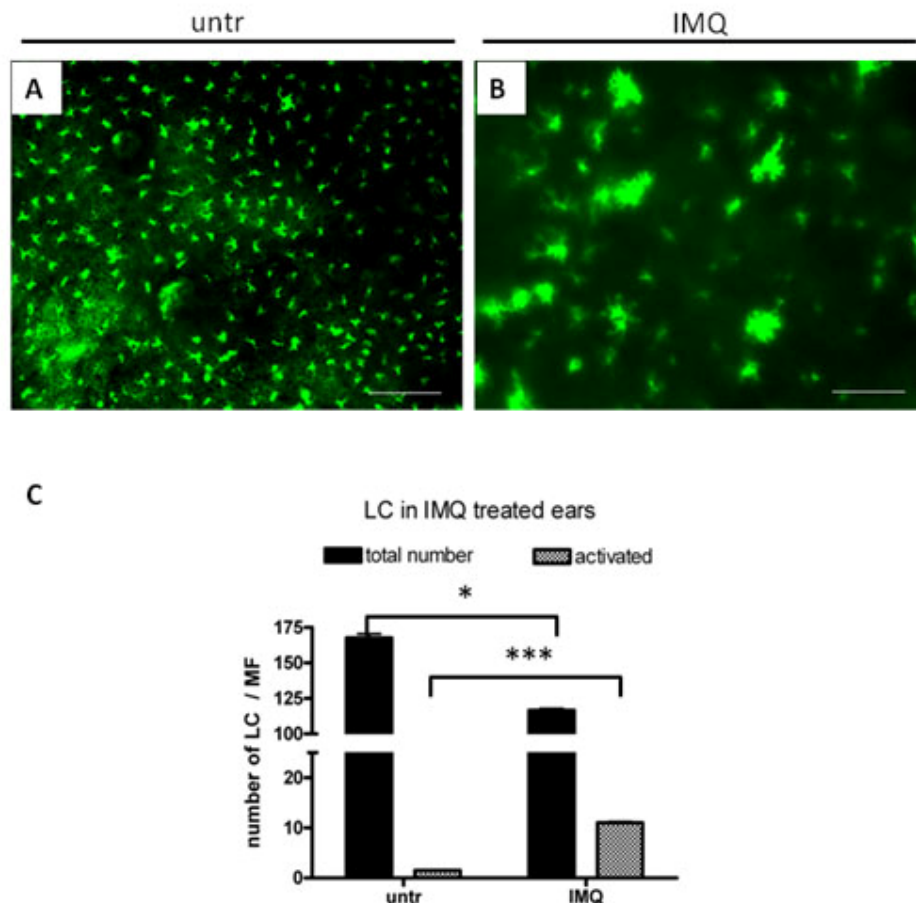
Fig. 10: Imiquimod leads to activation and emigration of Langerhans cells from mouse ears after 7 days of consecutive Aldara-treatment. A, B: epidermal ear sheets from untreated (A) and Imiquimod treated (B) mice stained for Langerin; C: quantification of total LCs and percentage of activated LCs. n = 3; scale = 100µm
Green: Langerin

FACS analysis also showed infiltration of several new immune cell populations, especially myeloid cells expressing the CD11b and CD11c surface molecules, as well as cells expressing mPDCA-1 and Ly6C into Imiquimod-treated ears (figure 11).
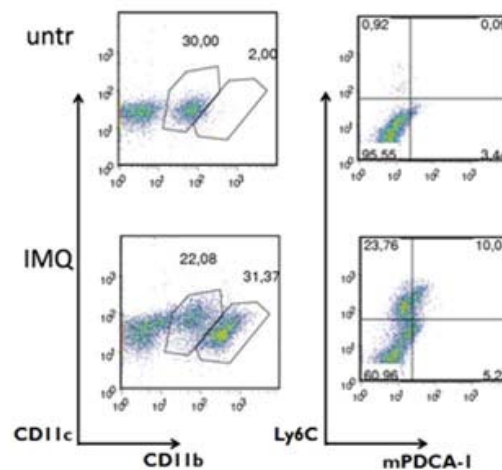
Fig. 11: FACS plots showing stainings for CD11b, CD11c, Ly6C, and mPDCA-1 from 7 days untreated and Imiquimod-treated adult WT mouse ears, gated on CD45 positive hematopoietic cells. It is shown that Imiquimod treatment leads to infiltration of CD11b$^+$, Ly6C$^+$ and mPDCA-1$^+$ cells into the dermis of mouse ears.

These findings confirm that LCs of C57BL/6 mice react to topical Imiquimod application and may lead to immune cell recruitment to the site of treatment. To investigate, whether the infiltrative effect of Imiquimod is altered in the absence of LCs in the epidermis, *LangerinDTR:EGFP* mice were depleted of LCs and creamed with Aldara on ears for seven consecutive days. The skin infiltrate was then analyzed by FACS to determine if an immune cell infiltrate can be observed in LC depleted mouse skin after Imiquimod treatment.

Imiquimod treatment results in an infiltrate of monocytes into the dermis. I could observe that in the absence on LC this infiltrate of CD11b+Gr-1+CD115+ cells was more than doubled (Fig.12A). Additionally, the number of CD8ε+ cells infiltrating into the skin was increased compared to mice treated with Imiquimod in the presence of LC. These CD8 ε + cells were mainly MHCII+ and only few of them were CD8 ε + T-cells (Fig.12B). No impact on the infiltrate of pDC like cells could be observed in the absence of LC. These results demonstrate that immunomodulatory effects of Imiquimod are not dependent on the presence of LCs in the epidermis.
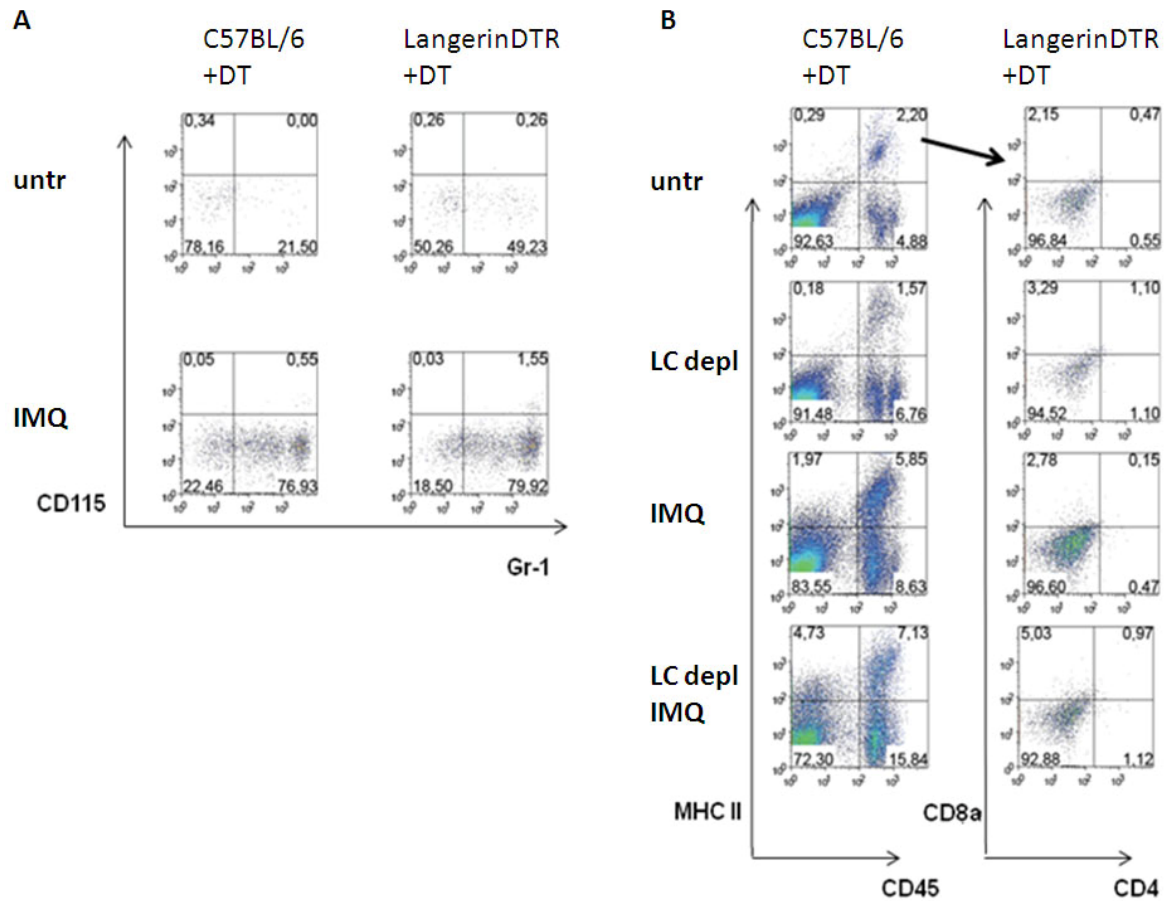
Fig.12: Flow cytometric analysis of skin cell suspensions. A: increased number of CD115/Gr-1 DP cells in LC depleted, Imiquimod treated skin; gated on CD11b high hematopoietic cells. B: Increased number of MHC II+ cells in Imiquimod treated skin (left). Among these there is a higher percentage of CD8ε+ cells in LC depleted, Imiquimod treated skin (right, gated on MHCII / CD45 DP cells).

To further analyze the effect of LCs on skin cancer growth and during skin cancer treatment with Imiquimod, I made use of the *LangerinDTR:EGFP* mouse model intradermally injected with B16F10 melanoma cells.

3.2 Effect of LCs on B16F10 melanoma growth

3.2.1 Tumor growth

In case of skin cancer, the Imiquimod induced immune cell infiltrate may lead to an effective killing of tumor cells, resulting in stagnation or even regression of tumor growth (Palamara 2004). To address the question, whether LCs contribute to the Imiquimod effect, $3.5 \cdot 10^4$ B16F10 melanoma cells per mouse were intradermally injected into *LangerinDTR:EGFP* knock-in mice. Mice were separated into four experimental groups: (1) untreated; (2) LC-depleted by DT injection; (3) Imiquimod-treated; and (4) LC-depleted by DT injection and Imiquimod-treated. DT injections were started when tumors were about 3.5 mm in diameter with a concentration of 200ng of DT per mouse. DT injections were repeated every fourth day, to exclude a replenishment of the skin with Langerin$^+$ cells (dDCs as well as LCs) during tumor growth and/or Imiquimod-treatment. Aldara-treatment was started 1-2 days after LC depletion (when tumor size was about 4 – 4.5 mm in diameter), ensuring that DT- and Imiquimod-treated mice were already depleted of LCs when Imiquimod application occurred. Imiquimod application to tumor overlaying skin was performed every second day until mice were sacrificed. Tumor size was measured every second day to evaluate the growth rates of tumors from all four mouse groups (Fig. 13).
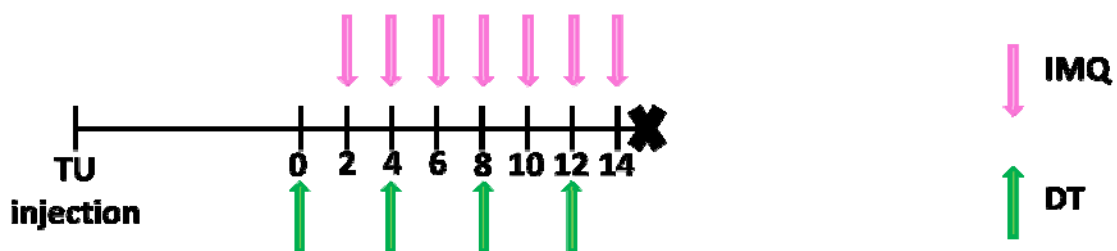
Fig. 13: Time scale of tumor treatment in the B16F10 melanoma model in *LangerinDTR:EGFP* mice.

Efficient depletion of LCs was confirmed by preparation of epidermal ear sheets stained for MHC class II molecules at the end of the experiment (figure 14). MHC-II negative sheets show an efficient depletion of Langerin$^+$ cells in the epidermis.
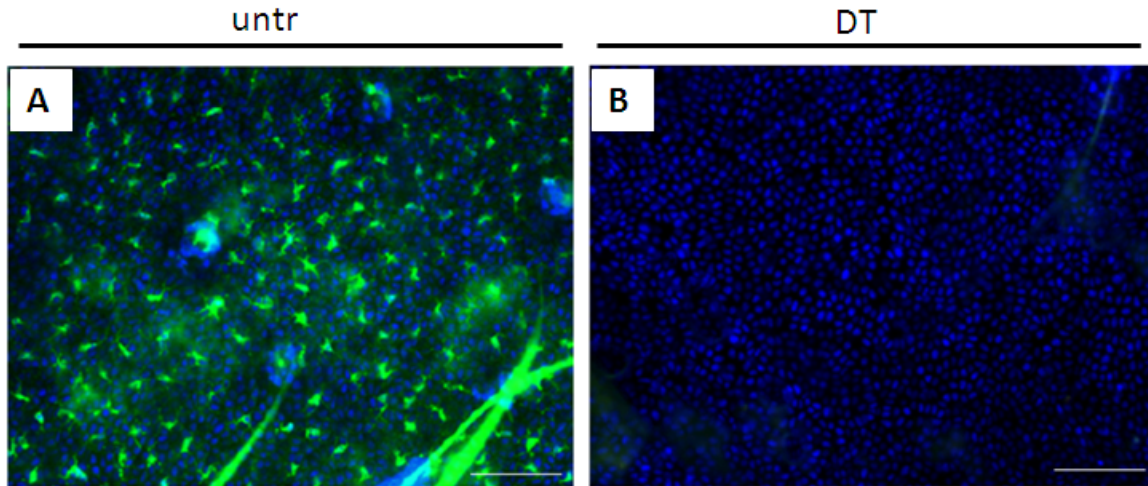
Fig. 14: LCs are efficiently depleted from the epidermis after DT treatment, confirmed by immunofluorescence staining of epidermal ear sheets 24-36 hours after the last injection of DT; A: untreated mouse; B: DT treated mouse. n = 4-7 mice of 2 independent experiments. scale = 100μm
Green: MHC-II; Blue: Hoechst

Tumor growth was not altered in LC-depleted mice compared to untreated WT mice, leading to the conclusion that LC function is not required to decelerate tumor proliferation. Imiquimod-treated WT mice showed a significantly slower tumor growth rate compared to untreated WT mice, showing that application of Aldara leads to an effective antitumoral reaction (figure 15). Interestingly, an Aldara effect was also observable in mice depleted of LCs and treated with Imiquimod compared to both untreated WT mice and LC-depleted mice. These findings suggest that Imiquimod acts in the absence of LCs and Langerin[+] dDCs.
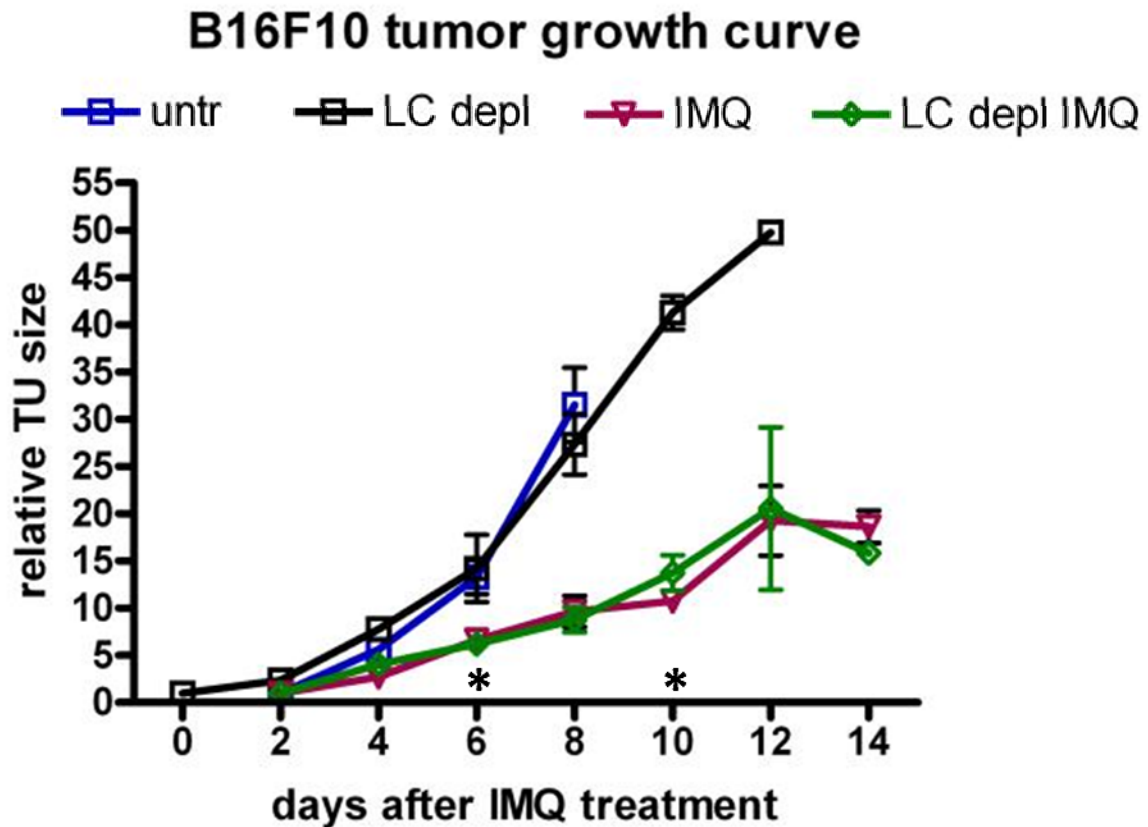
Fig. 15: LCs are not responsible for the mediation of the antitumoral effect of Imiquimod. Graphs shows B16F10 melanoma tumor growth curves in untreated (blue), LC depleted (black), Imiquimod treated (red) and LC depleted Imiquimod-treated (green) mice. Graph shows results of a representative experiment out of three independent experiments; n = 4-7 mice.

3.2.2 Immune cell infiltrate into B16 melanoma

It was reported previously from our lab, that different subtypes of immune cells are infiltrating the skin sites where Imiquimod is applied and also Imiquimod treated melanomas (Palamara 2004). To confirm these data in C57BL/6 mice for the B16F10 tumor model and to characterize the immune cell infiltrate into tumors of mice depleted of Langerin+ cells immunofluorescence stainings were performed on frozen sections, making use of several immune cell markers (figure 16).

Costaining of CD4 and CD3ε on sections from B16F10 tumors revealed considerably higher numbers of CD4 single positive (SP) cells compared to CD4/CD3ε double positive (DP) cells in all mice, indicating that most CD4$^+$ infiltrating cells were not

CD4$^+$ T cells (figure 16A,D,G,J). Indeed, Imiquimod-treated WT mice showed a significantly increased CD4$^+$ cell infiltrate compared to untreated WT mice. Interestingly, although an Aldara effect was observed, an increased CD4$^+$ cell infiltrate could not be detected in LC-depleted Imiquimod-treated mice (figure 17A). Among the CD4/CD3ε DP T cells there were no differences in infiltrating cell numbers detectable (figure 17B).

To detect, whether the CD3ε$^-$/CD4$^+$ cells were DCs, costaining of MHC-II and CD4 was performed (figure 16B,E,H,K). Imiquimod-treated WT mice showed a significant increase in infiltrating CD4/MHC-II double-positive cells compared to LC-depleted Imiquimod-treated mice (figure 17C). This finding indicates that LCs are required for recruitment of CD4/MHC-II double-positive (DP) cells to the site of Aldara application, but that these DP cells do not seem to be important for the Imiquimod effect on tumor growth.

Since recent publications showed that Imiquimod treatment leads to massive infiltration of CD8$^+$ T cells into human skin cancer, followed by tumor clearance, immunofluorescence costainings of CD8 and CD3ε were performed on frozen sections of B16F10 tumors (figure 16C,F,I,L). Quantification of the total number of CD8$^+$ cells revealed comparable numbers among all four mouse groups (figure 17D). However, Imiquimod treated WT mice showed higher CD8$^+$ T cell numbers in B16F10 melanoma compared to untreated WT controls. This increase could not be observed in the absence of Langerin$^+$ cells since CD8$^+$ T cell numbers in Aldara treated WT mice were also higher than in tumors from LC-depleted Imiquimod treated mice (figure 17E). From these data it may be concluded that Langerin$^+$ cells seem to be required for priming of cytotoxic CD8$^+$ T cells. Surprisingly, like for CD4/MHC-II DP cells, the influx of CD8/CD3ε DP cells into the tumors does not seem to be essential for Imiquimod dependent reduced tumor growth.
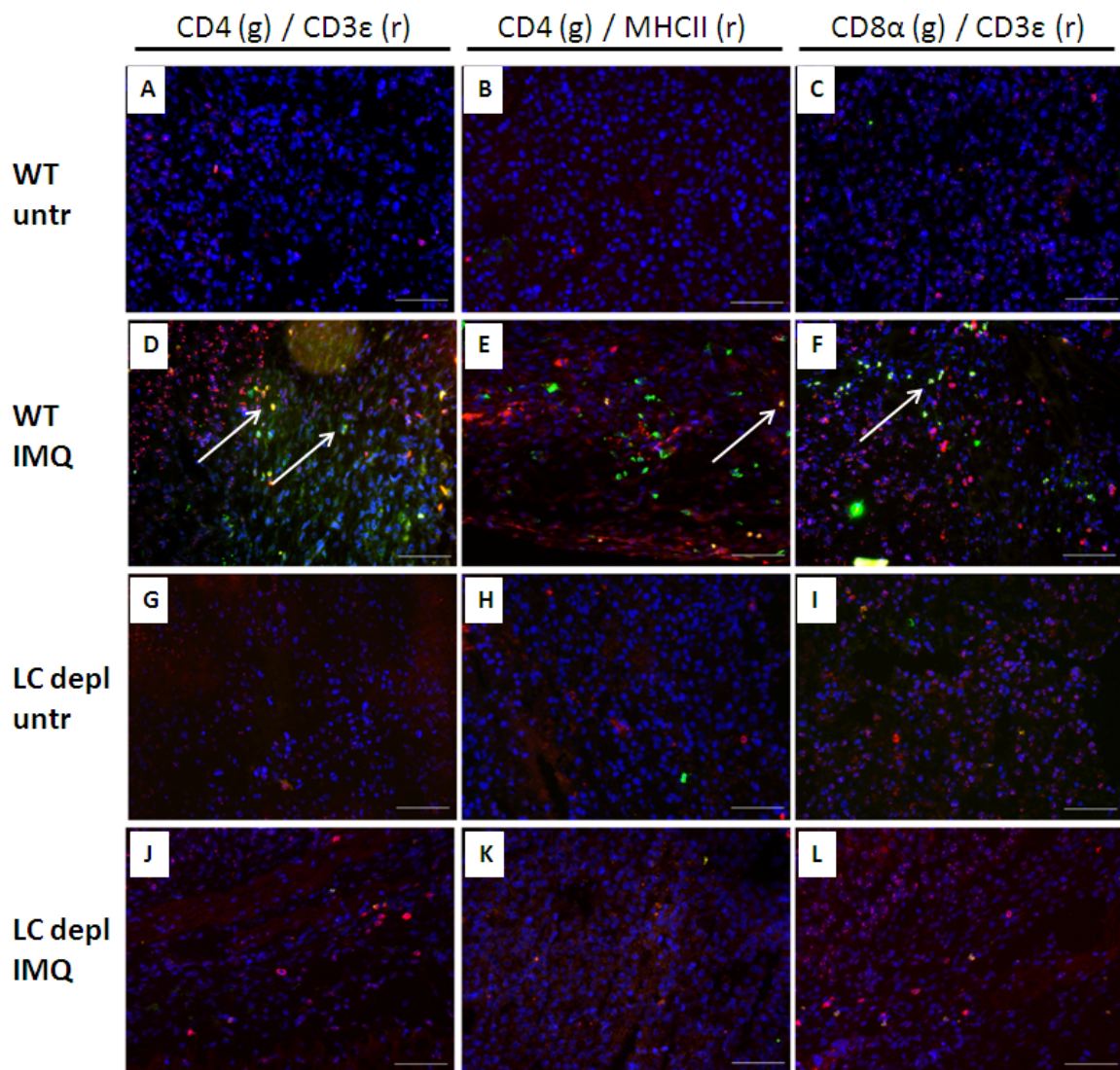
Fig 16: Langerhans are required for recruitment of MHCII/CD4 DP and CD8+ T cells into B16F10 tumors upon Imiquimod application to tumor overlaying skin. A, B, C: tumor sections from B16F10 bearing untreated WT mice; D, E, F: tumor sections from B16F10 bearing Imiquimod treated WT mice; G, H, I: tumor sections from B16F10 bearing LC-depleted mice; J, K, L: tumor sections from B16F10 bearing Imiquimod treated LC-depleted mice. scale = 100μm, arrows pointing on double positive cells in the respective staining:

A, D, G, J – Green: CD4, Red: CD3e, Blue: Hoechst

B, E, H, K – Green: CD4, Red: MHCII, Blue: Hoechst

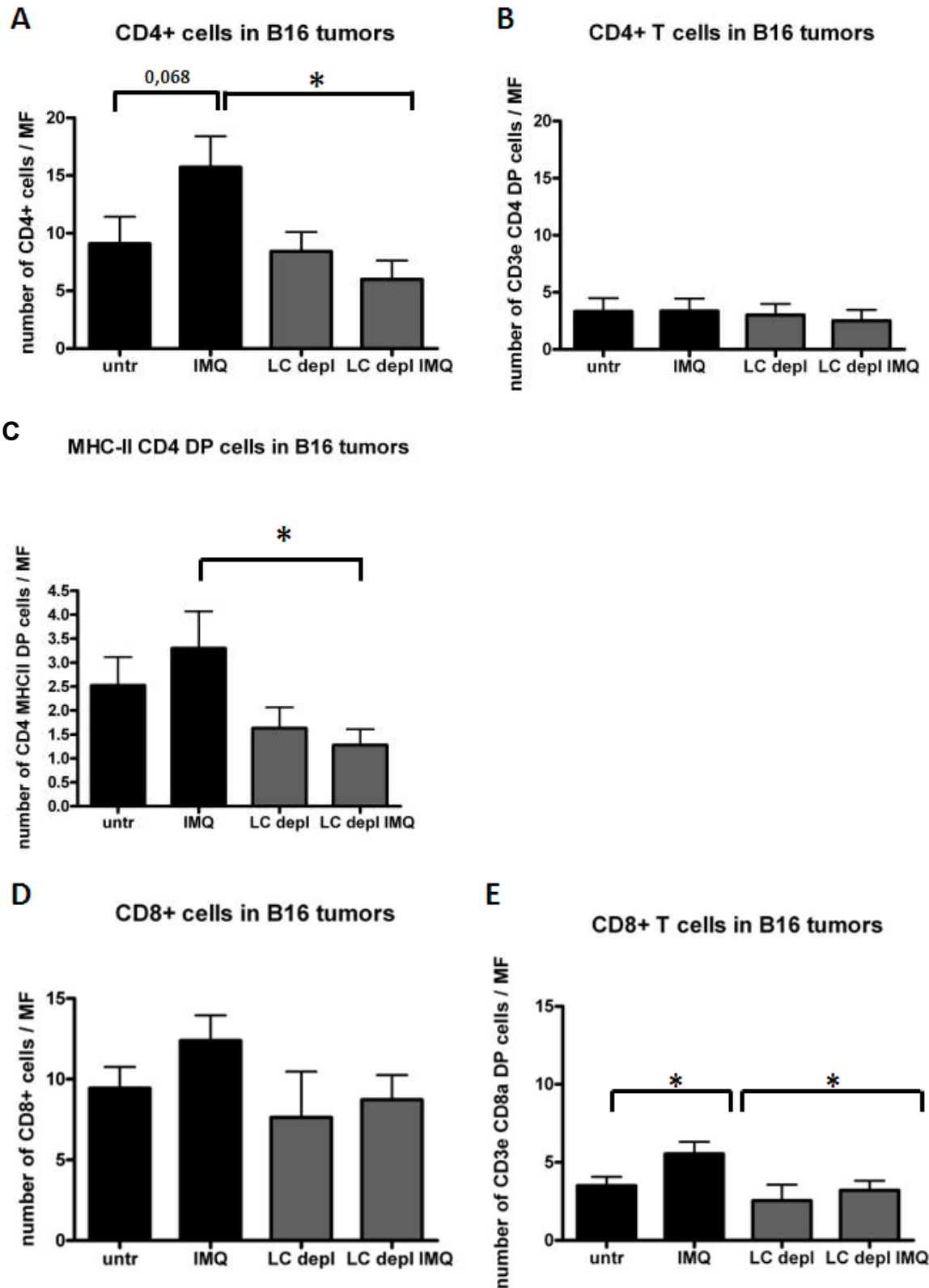C, F, I, L – Green: CD8a, Red: CD3e, Blue: Hoechst

Fig. 17: Quantification of cellular composition of the immune cell infiltrate of B16F10 melanoma grafted tumors. A: CD4 SP cells; B: CD4^{+} T cells; C: MHCII CD4 DP cells; D: CD8 SP and E: CD8^{+} T cells. n = 4-7 mice of 2 independent experiments.

3.2.3 Skin morphology and mast cell infiltration

I have shown that Imiquimod acts on melanoma growth in mice even in the absence of LCs although the immune cell infiltrate is perturbed. To better understand the mechanism of action of Imiquimod in the absence of LCs I took a closer look at the direct effects of Imiquimod on the skin.

Histological stainings with H&E showed epidermal thickening in mouse skin treated with Imiquimod, independently of the presence of LCs (figure 18A,C,E,G). Both, WT and LC depleted Imiquimod treated mice exhibited a significant increase in epidermal thickness compared to their untreated counterparts (figure 19A). This result indicates a direct action of Imiquimod on keratinocytes, thereby leading to acanthosis.

A recent study (Schild 2007) showed that the function of Imiquimod is exerted by activation of mast cells. Activated, degranulating mast cells in turn are claimed to activate LCs. Giemsa stainings performed on paraffin sections of B16F10 tumor overlaying skin (figure 18B,D,F,H) confirmed that tumor overlaying skin in all Imiquimod treated mice contained increased numbers of mast cells, independently of the presence of LCs (figure 19B). Imiquimod-treated WT mice showed a trend towards increased degranulation of mast cells compared to untreated control animals, but this difference was statistically not significant. In contrast, LC-depleted Imiquimod-treated mice showed statistically significant higher rates of degranulated mast cells compared to untreated LC-depleted controls (figure 19C). Putting these data together Imiquimod seems to stimulate mast cells to degranulate. This reaction might be antagonized by LCs, thereby influencing the immunogenicity of the inflammatory environment.

Taking all data together, it can be concluded, that LCs are not the mediators of the anti-tumoral effect of Imiquimod. B16F10 tumor growth is reduced in Imiquimod treated LC-depleted mice in the same extent as it is observed in LC-containing control mice. Although absence of LCs from the epidermis seems to result in a reduced recruitment of CD8$^+$, CD4$^+$ and MHC-II/CD4 DP cells to the skin when compared to WT mice. The lack of these tumor infiltrating immune cells does not seem to impair the anti-tumoral action of Imiquimod.
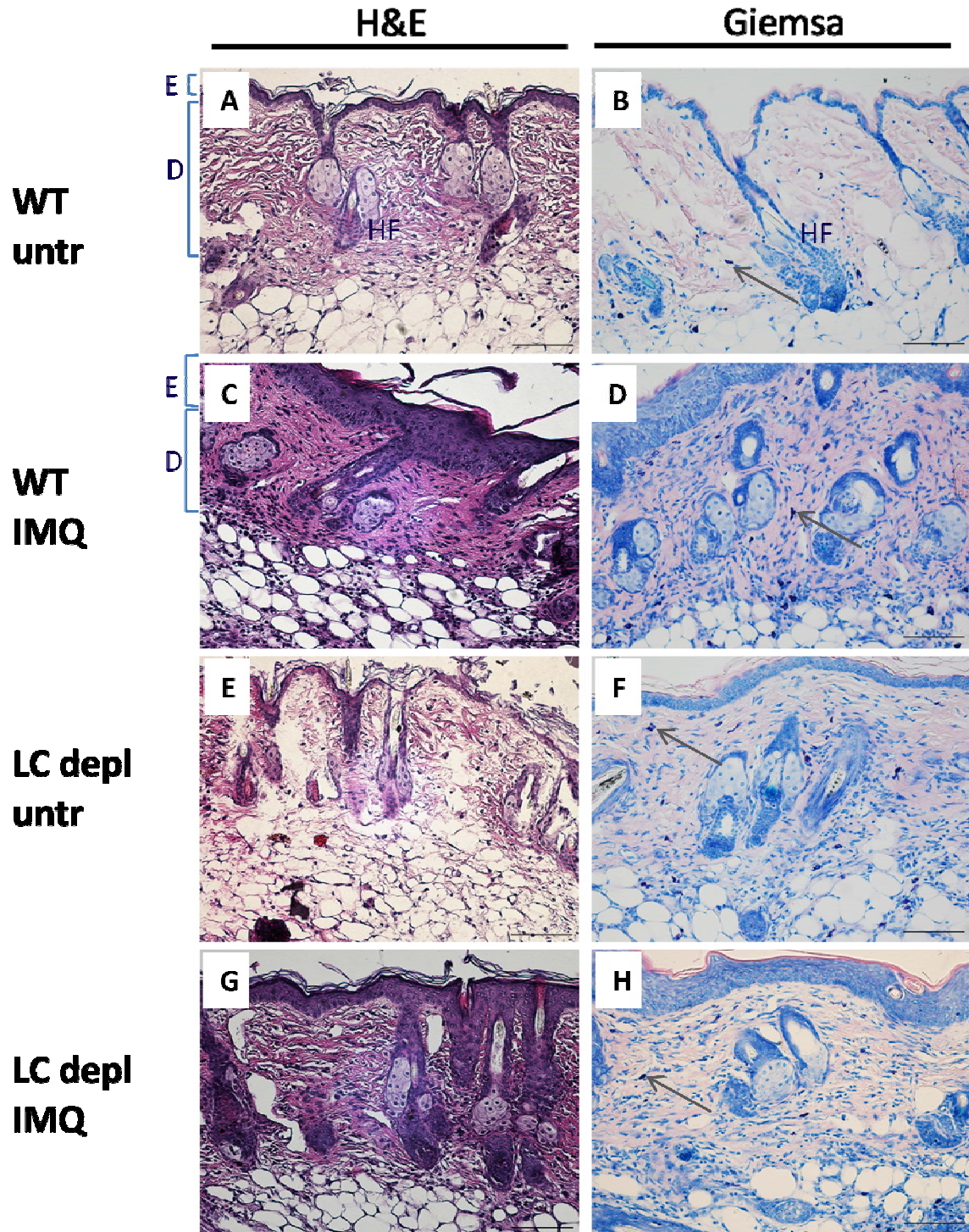
Fig. 18: Morphology and mast cell numbers of tumor overlaying skin from B16F10 grafted LangerinDTR:EGFP mice. A, C, E, G: Histological stainings with H&E; B, D, F, H: histological stainings using Giemsa stain, grey arrows pointing on mast cells. scale = 100µm
Abbreviations: E – epidermis; D – dermis; HF: hair follicle
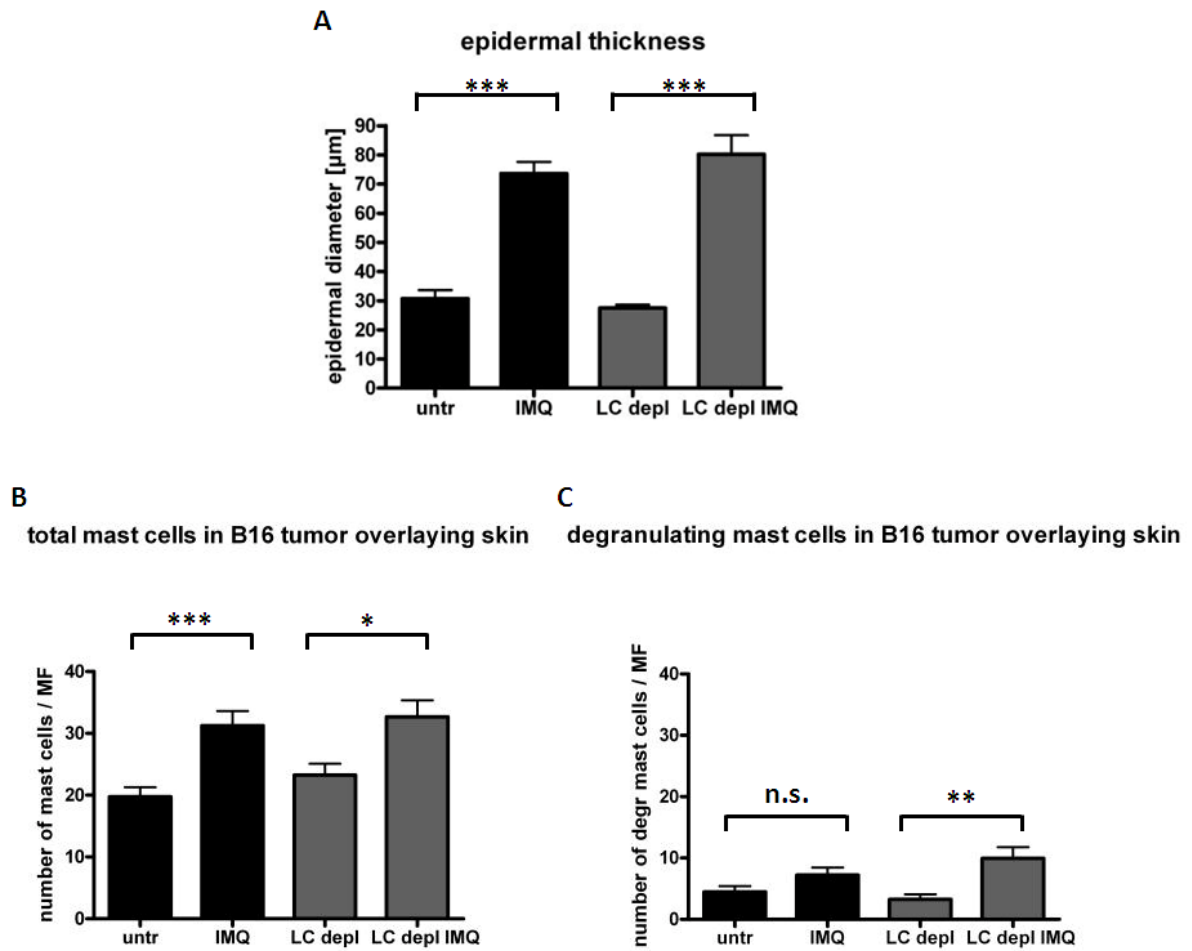
Fig 19: Histological analysis of tumor overlaying skin from B16F10 tumor bearing LangerinDTR:EGFP mice. A: Quantification of measurement epidermal thickness, B: quantification of total skin mast cell numbers; C: counts of degranulated skin mast cells.

3.3. Influence of presence of BCC on skin microenvironment

3.3.1 Breeding and treatment of mice

Imiquimod is most successfully used in humans to treat BCC. To develop a model, where the mechanisms underlying the successful therapy of BCC using Imiquimod can be studied, I utilized an inducible model of BCC by first crossing $SmoM2YFP^{fl/fl}$ mice to $K5Cre^{ERT}/+$. These $SmoM2YFP^{fl/fl}$ $K5Cre^{ERT}/+$ mice were further crossed to $LangerinDTR:EGFP$ mice to generate $SmoM2YFP^{fl/+}$ $K5Cre^{ERT}/+$ $LangerinDTR:EGFP$ mice (further referred to as $SmoM2LangerinDTR$ mice), which allow to study the role of LCs in BCC development and progression. Goal of the initial experiments was to establish protocols for BCC-induction and to address whether BCC-treatment with Imiquimod in LC containing $SmoM2LangerinDTR$ mice is comparable to treatment in humans.

Induction of Cre-recombination was performed according to the published protocol (Mao 2006), starting at postnatal day 10 (P10) by injection of tamoxifen for 5 consecutive days, leading to expression of $smoM2$. Mice were continuously given tamoxifen once a week after induction of Cre expression. At ~ day 45 neoplastic changes could be observed microscopically in the skin of $SmoM2LangerinDTR$ mice (data not shown), whereas macroscopically visible BCC lesions developed by day 80 to day 90. Therefore the timepoint of day 90 was chosen to start Aldara treatment of BCC. Analogous to the human schedule, mice were treated for 5 consecutive days with Imiquimod (Aldara patient package insert 2009), followed by two days of recovery, followed by 5 days of treatment (figure 20). As in mice BCC is most prominently visible at ears and tail, ear biopsies were taken at day 90 (further indicated as experimental day 0), and were compared to ear biopsies obtained at the end of the experiment (experimental day 12). Ears of both timepoints were then compared to monitor disease progression in untreated and Aldara-treated mice. After the second week of Aldara application, photographs of ears and tails were taken and mice were sacrificed at experimental day 12 (figure 21).

Due to a lack of time during the thesis, no LC depletion experiments could be performed during this project. It is still necessary to evaluate the effect of LC presence on BCC growth, but also on BCC development. Therefore DT injections need to be started at different timepoints: for investigating the role of LCs on BCC growth LC depletion needs to be initiated by day 88. Analyzing the effect of LCs on BCC development requires LC depletion starting by day 10.
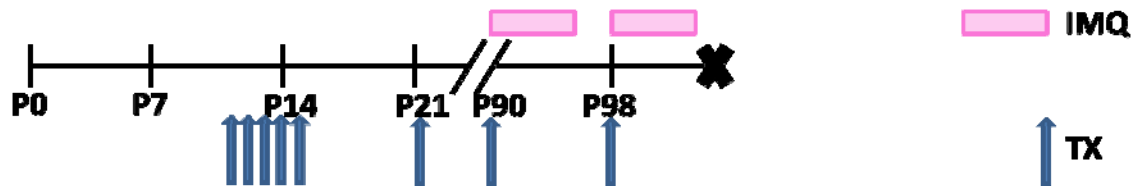
Fig. 20: time schedule of BCC induction by tamoxifen in *SmoM2LangerinDTR* mice and Imiquimod treatment.

To analyze BCC growth during my thesis, I processed the skin of ears and tails for histological analysis and characterized these tissue biopsies by immunofluorescence stainings, H&E and Giemsa stainings.

Macroscopical analysis of BCC bearing mice showed that severity of BCC was diverging from individual to individual (figure 20). It also indicated that Imiquimod treatment for 2 weeks did not lead to disease clearance, as BCC lesions were still visible on ears and tails of *SmoM2LangerinDTR* mice.
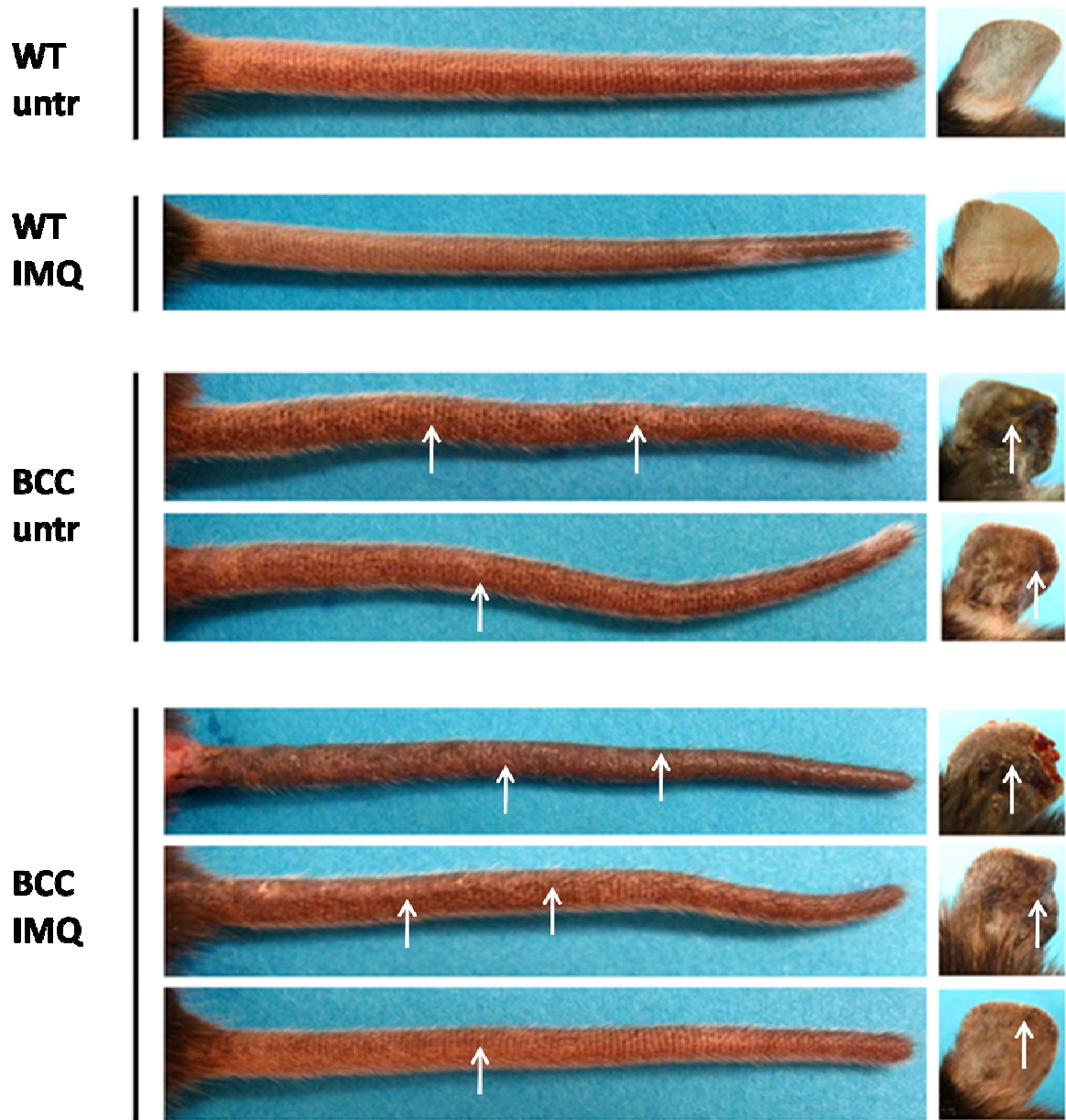
Fig. 21: Macroscopioc images from ears and tails of healthy and BCC bearing mice at experimental day 12; arrows showing BCC lesions in age matched SmoM2LangerinDTR mice. n = 2-3 of 2 independent experiments.

3.3.2 Skin morphology and skin mast cell infiltration

Figure 22 shows H&E stainings from ear sections of unaffected and BCC bearing mice. Healthy *SmoM2LangerinDTR* mice treated with Imiquimod show signs of acanthosis on day 12 (figure 22A-D), indicating that Imiquimod has acted properly on BCC unaffected skin.

In the third row an ear section of untreated *SmoM2LangerinDTR* mice is shown, demonstrating branched basal cell layer protrusions into the dermis, accompanied by increased melanocyte location to BCC formations (figure 22E-H, indicated by green arrows). Neoplastic morphological changes of the basal cell layer are most obvious in interfolicular epidermis and the infindibulum. Furthermore the epidermis in BCC bearing *SmoM2LangerinDTR* mice exhibits an increase in diameter compared to healthy epidermis (figure 23). Large blood vessels can also be noticed in close proximity to foci of neoplastic skin (figure 22E-H). Comparison of skin morphology of experimental day 0 and day 12 shows that neoplastic foci of untreated, as well as of Imiquimod treated BCC bearing mice are increasing over time (figure 22E-H). The progression of BCC growth is accompanied by melanocyte aggregation in the dermis. BCC bearing mice treated with Imiquimod still harbor neoplastic lesions in their skin at day 12, showing that the disease is not regressing after a 2 week treatment.

Like in the B16F10 melanoma experiments, an effect of Imiquimod treatment on epidermal thickness can be observed: application of Aldara leads to induction of acanthosis. Aldara creamed ears show significantly increased epidermal thickness at day 12 compared to day 0 after treatment in healthy and in BCC bearing *SmoM2LangerinDTR* mice (Fig. 17C-D, 17G-H). This indicates that Aldara exerts keratinocyte activating function not only in normal, but also in BCC affected skin.
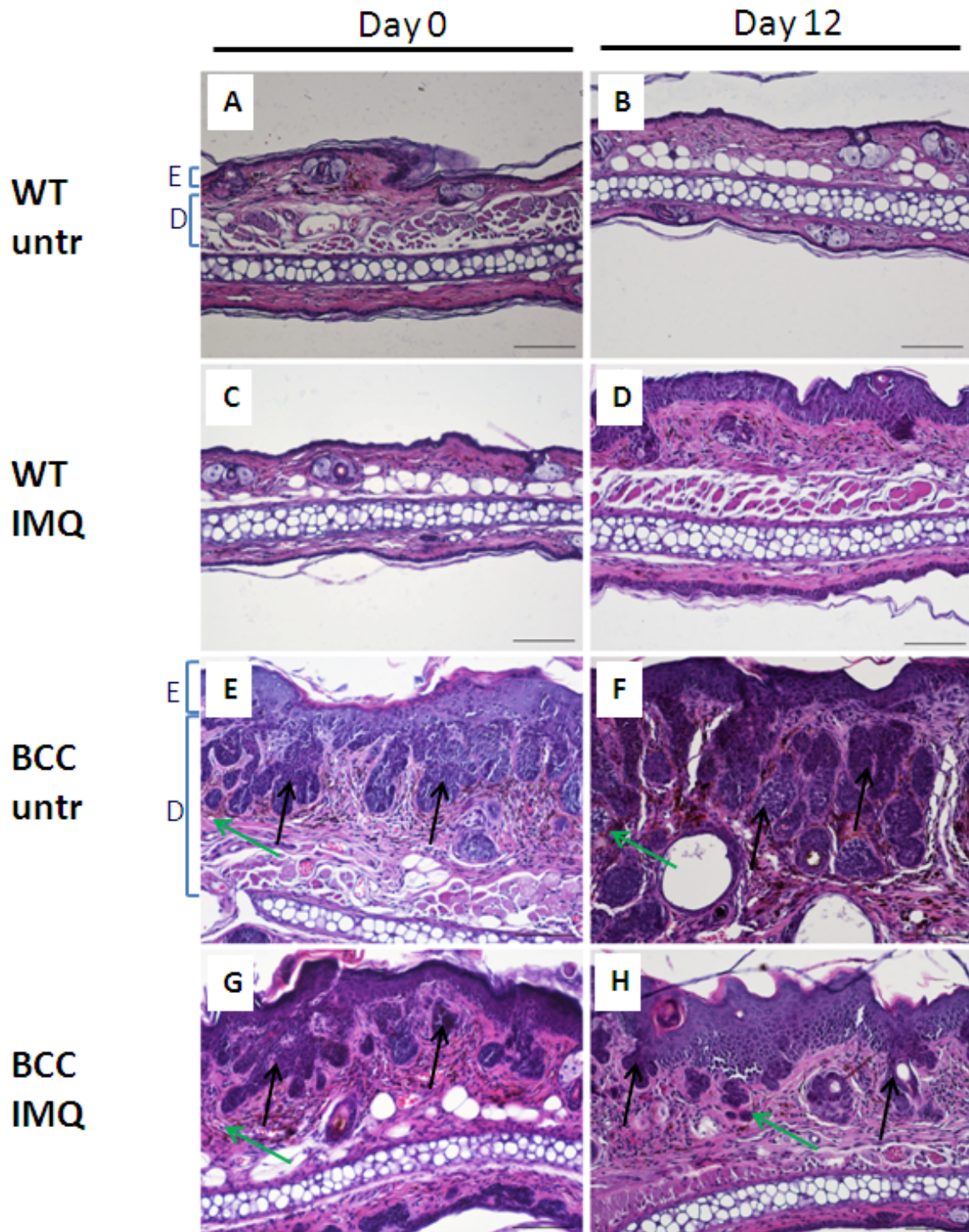
Fig. 22: skin morphology of healthy and BCC bearing mouse ears. Imiquimod treatment for 2 weeks does not lead to regression of BCC. A, C, E, G: H&E stainings of ear sections on experimental day 0; B, D, F, H: H&E stainings of ear sections on experimental day 12, green arrows indicating melanocytes, black arrows indicating basal-cell carcinoma like structures branching into to dermis. scale = 100µm

Abbreviations: E- epidermis, D – dermis

epidermal diameter in BCC
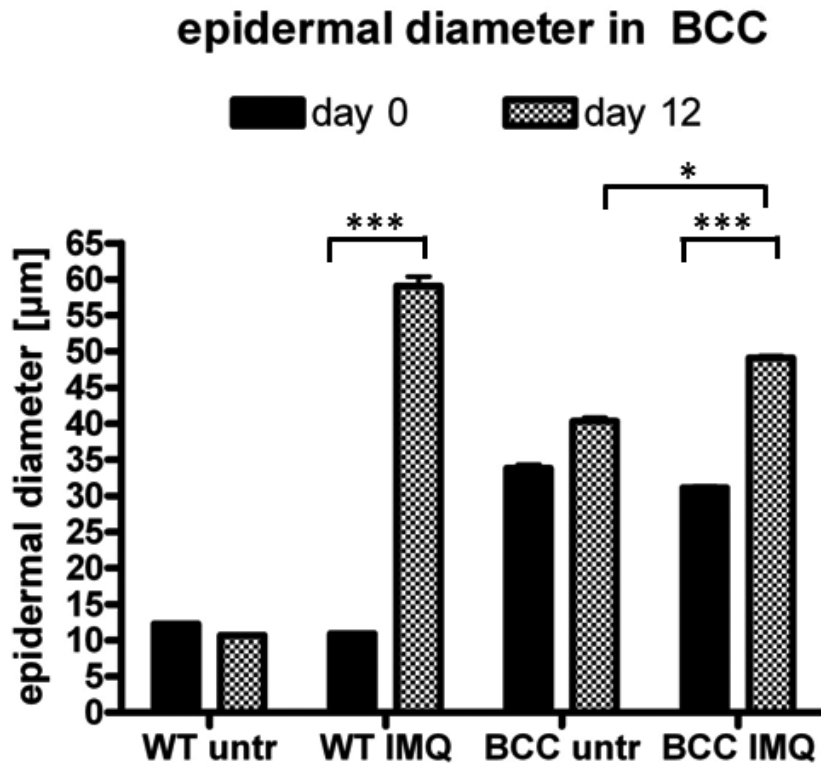
Fig. 23: diagram of measurement of epidermal thickness in healthy and BCC bearing mice comparing experimental day 0 amd day 12. n = 2-3 mice per group.

As H&E stainings of BCC bearing ears showed an infiltrate into the dermis, I further wanted to analyze, whether presence of BCC or Imiquimod treatment have an effect on mast cell numbers and degranulation in this tumor model. Giemsa stainings reveal increased numbers of total and activated mast cells in ear skin of untreated BCC bearing mice compared to untreated WT animals (figure 24A-B, 24E-F). This indicates that BCC progression leads to mast cell infiltration and degranulation. BCC unaffected *SmoM2LangerinDTR* mice treated with Imiquimod for 12 days exhibit significantly increased numbers of activated mast cells compared to day 0. In contrast, BCC affected skin contains more mast cells independently of Imiquimod application (figure 25). Therefore I conclude that Imiquimod application does not affect mast cell degranulation in presence of BCC. Whether this is due to release of anti-inflammatory factors from keratinocytes or to suppressive function of Imiquimod-induced infiltrating immune cells is under investigation.
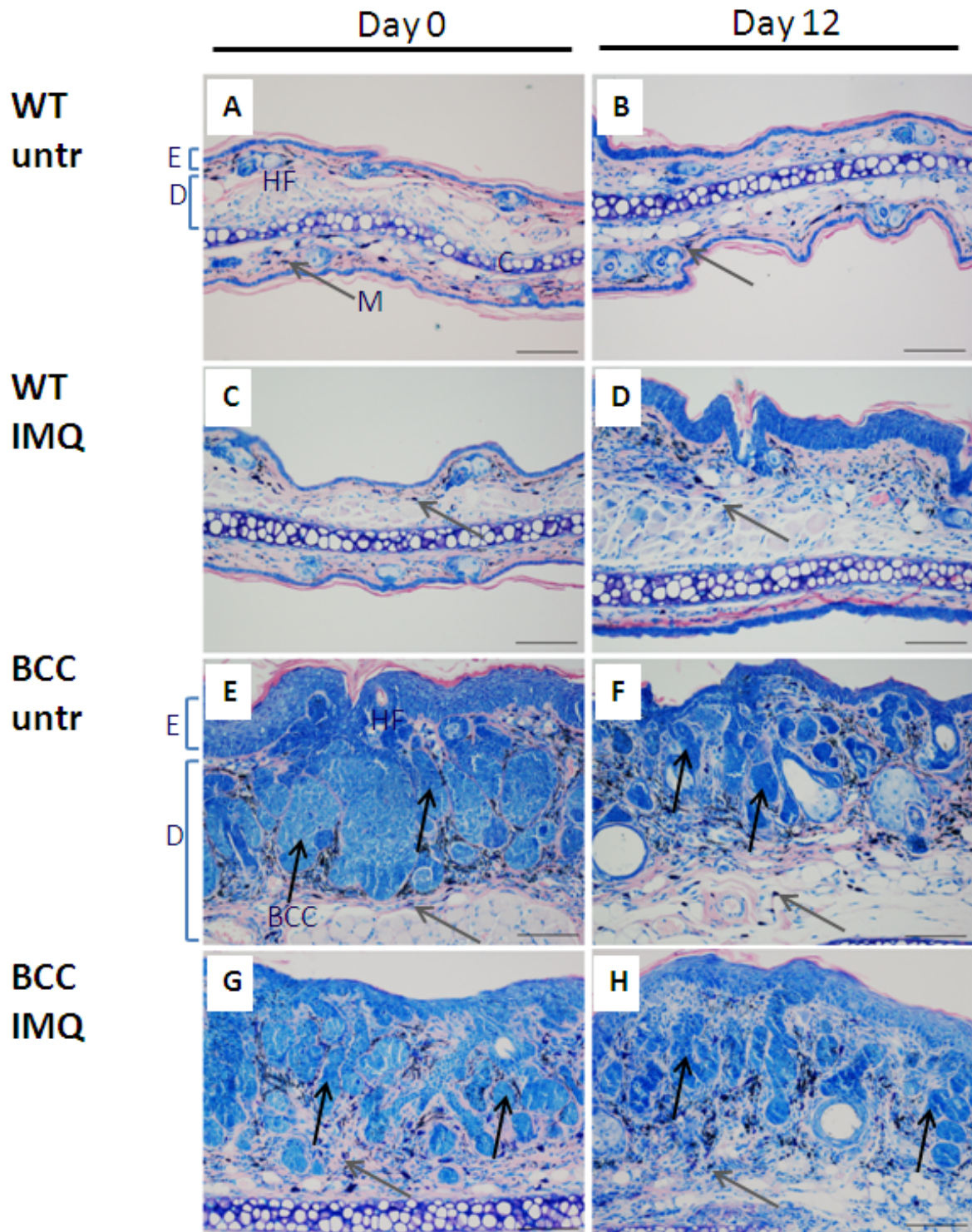
Fig. 24: Giemsa staining on histological sections of healthy and BCC bearing mouse ears. Presence of BCC leads to increased mast cell numbers. A, C, E, G: Giemsa stainings of ear sections on experimental day 0; B, D, F, H: Giemsa stainings of ear sections on experimental day 12, grey arrows indicating mast cells, black arrows indicating basal-cell carcinoma like structures branching into to dermis. scale = 100µm

Abbreviations: E- epidermis, D – dermis, HF – hair follicle, M – mast cell, C – cartilage

A

total skin mast cells

■ day 0　▨ day 12

number of total mast cells / MF

B

activated skin mast cells

■ day 0　▨ day 12

number of activated mast cells / MF
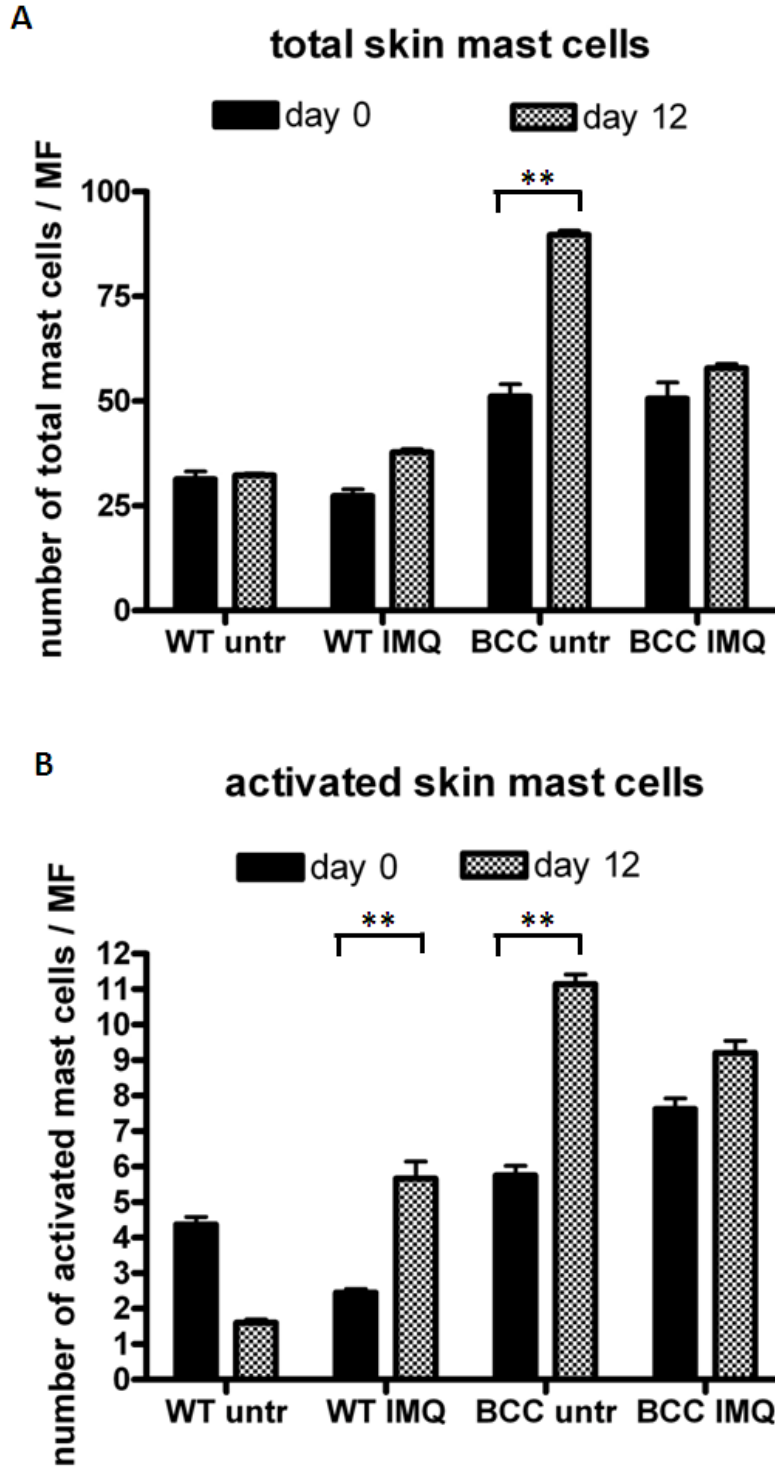
Fig. 25: total number of mast cells as well as degranulated number of mast cells increases after 2 weeks in untreated BCC bearing mice. A: quantification of total mast cell numbers in ear skin of healthy and BCC bearing mice;　B: quantification of degranulated mast cell numbers in ear skin of healthy and BCC bearing mice. n = 2-3 mice per group.

3.3.3 Epidermal LC distribution

Several recent publications show an alteration of epidermal immune cell distribution in human skin affected by BCC (Santos 2010, Mardones 2009). These studies claim a high density of LCs in peritumoral areas, whereas LCs seem to be absent from tumor overlaying skin. To investigate, if this phenomenon is also seen in the SmoM2LangerinDTR mouse model, immunofluorescence staining using antibodies against Langerin and MHC-II was performed on epidermal ear sheets at day 0 from unaffected and BCC affected mice (figure 26A-B). Morphological differences of LCs between WT and BCC bearing mice can be seen – LCs in BCC bearing ears appear smaller in contrast to LCs from unaffected skin. Second, like in humans, a rearrangement of the LC network in BCC affected skin is observable – LCs from BCC bearing ears partially cluster and show a decrease in the intensity of MHC-II expression. In some areas of the ear keratinocytes of BCC bearing mice exhibit expression of MHC-II (figure 26B). These areas are considered to be inflamed. LC allocation in BCC affected *SmoM2LangerinDTR* ear epidermis shows striking differences between MHCII$^+$ keratinocyte areas and MHC-II$^-$ keratinocyte areas: LC density in MHCII$^+$ keratinocyte areas is increased, whereas it is found to be decreased in MHCII$^-$ keratinocyte areas (figure 26C). These results indicate that keratinocytes are inflamed and that LCs are activated and redistributed in BCC affected skin.
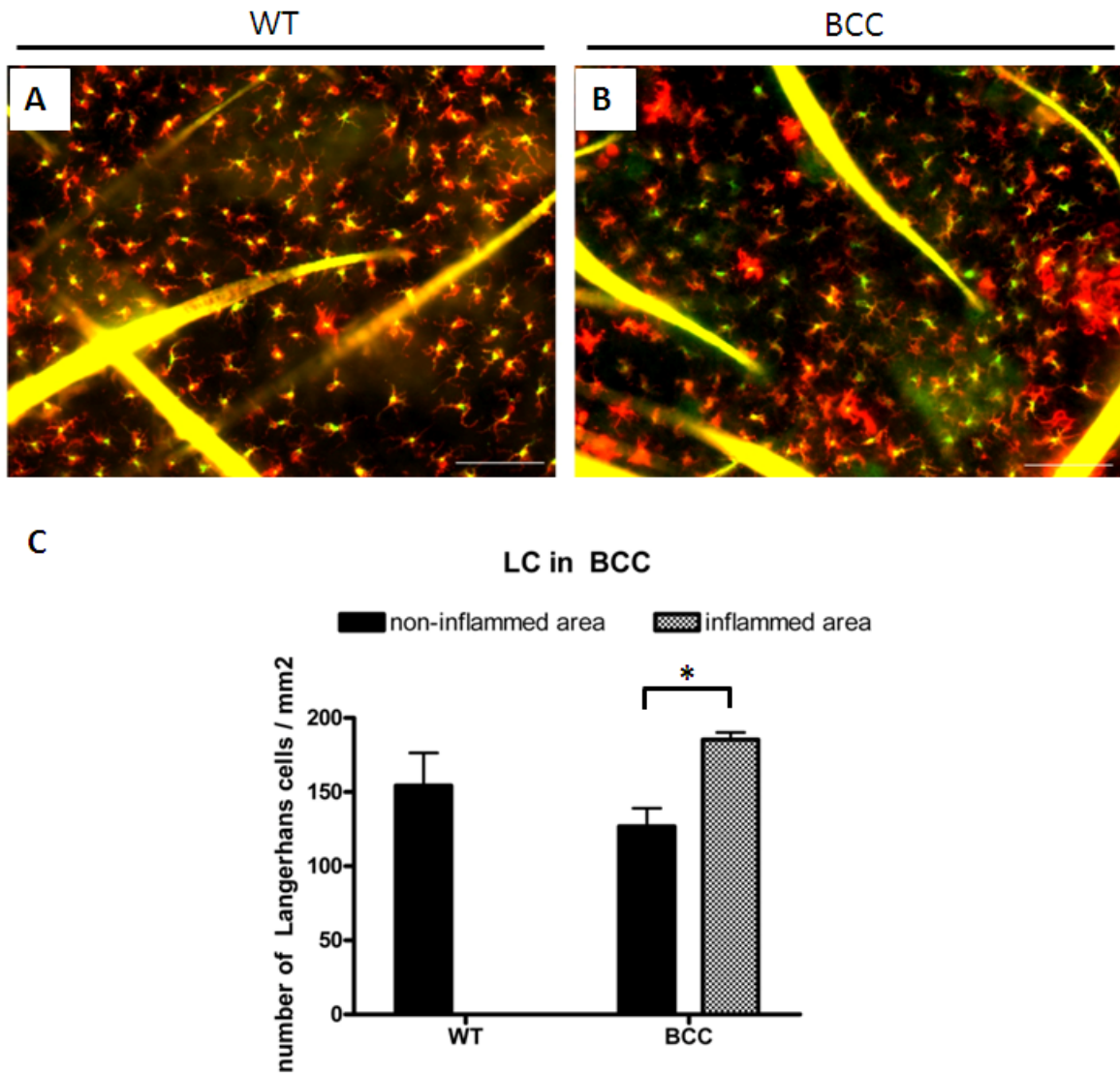
Fig. 26: LCs are redistributed in the epidermis of BCC bearing mice compared to healthy mice.
A: immunofluorescence staining of ear sheets, showing a representative healthy mouse ear, B:
immunofluorescence staining of ear sheets, showing a representative BCC bearing mouse ear;
C: quantification of LCs in ear areas of keratinocytes negative or positive for MHCII. n = 2-3
mice per group. scale = 100μm
Green: Langerin; Red: MHC-II

3.3.4 Immune cell infiltration into skin

The finding of redistribution of activated epidermal immune cells can also be seen in immunofluorescent stainings on cryosections from ears of *SmoM2LangerinDTR* mice (figure 27, 28). According to disease severity skin areas were classified into "strong" and "mild" BCC. As already seen in *en face* view on epidermal ear sheets from unaffected and BCC affected *SmoM2LangerinDTR* mice, cryosections showed different distribution of epidermal immune cells in BCC affected mice compared to WT mice. LCs, as well as γδ T cells were mostly absent from epidermal regions directly overlaying prominent BCC formations, whereas they were found in normal numbers in peritumoral (mildly affected) or healthy skin regions (figure 27B-C, figure 28B-C). These results suggest that similar to the human situation in the SmoM2LangerinDTR model peritumoral skin is inflamed and contains increased numbers of immune cells like LC and γδ T cells whereas in the skin directly overlaying the tumor immune cells are rather reduced (figure 27G, 28G).

This alteration of LC distribution is not influenced by application of Imiquimod (figure 27E-F, figure 28E-F).

The immunofluorescence staining also showed that development of BCC leads to infiltration of $CD3\varepsilon^+$ and $MHCII^+$ immune cells into the dermis. Microscopical analysis suggests that the intensity of infiltration is enhanced upon Aldara treatment (figure 27E, 28E). Imiquimod application onto healthy skin for 2 weeks is also accompanied by increased immune cell infiltration into the dermis (figure 27D, 28D). I therefore conclude, that in a 2 week Imiquimod treatment of BCC in the SmoM2LangerinDTR mouse model, Aldara application leads to an increased recruitment of $MHCII^+$ cells or T cells compared to untreated mice.
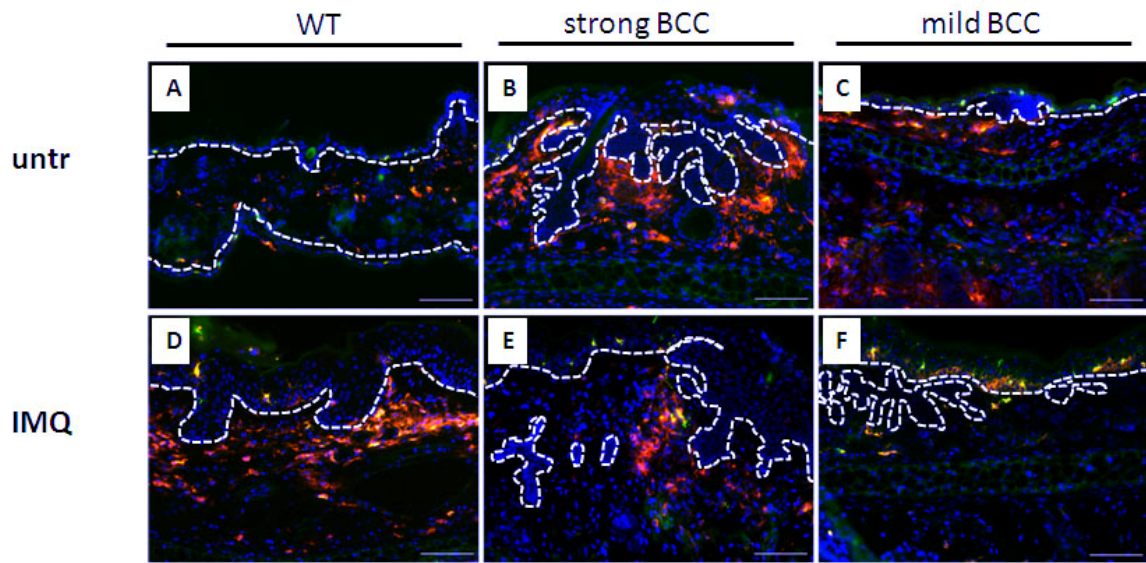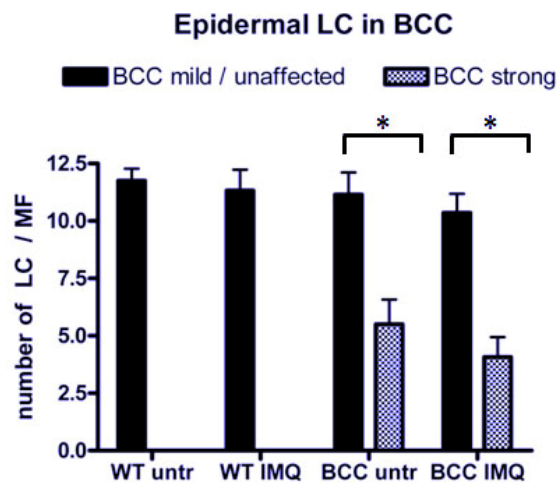
Figure 27: Distribution of LCs in BCC affected skin is altered: Immunofluorescence stainings on cryosections from healthy and BCC bearing mice treated and untreated with Imiquimod; A: untreated healthy mouse, B: untreated BCC showing a strong phenotype, C: untreated BCC showing a mild phenotype, D: Imiquimod treated healthy mouse ear, E: Imiquimod treated BCC showing a strong phenotype, F: Imiquimod treated BCC showing a mild phenotype; G: quantification of LC numbers in epidermis overlaying BCC of strong and mild phenotype. n = 2-3 mice per group. scale = 100µm
Green: Langerin; Red: MHCII; Blue – Hoechst
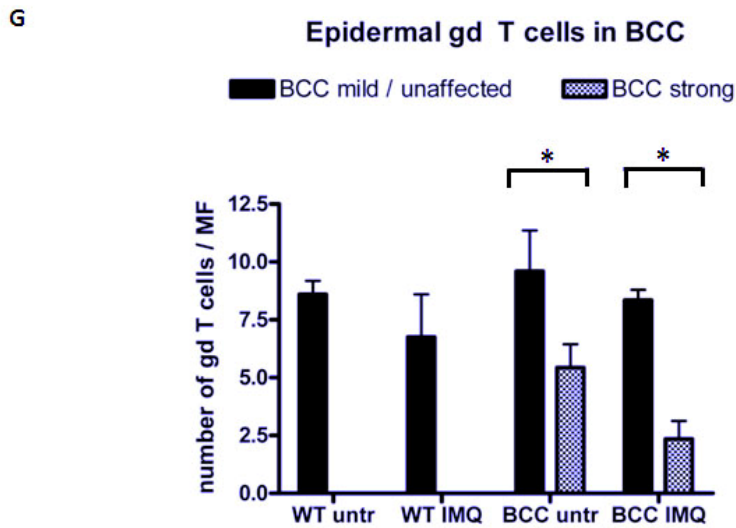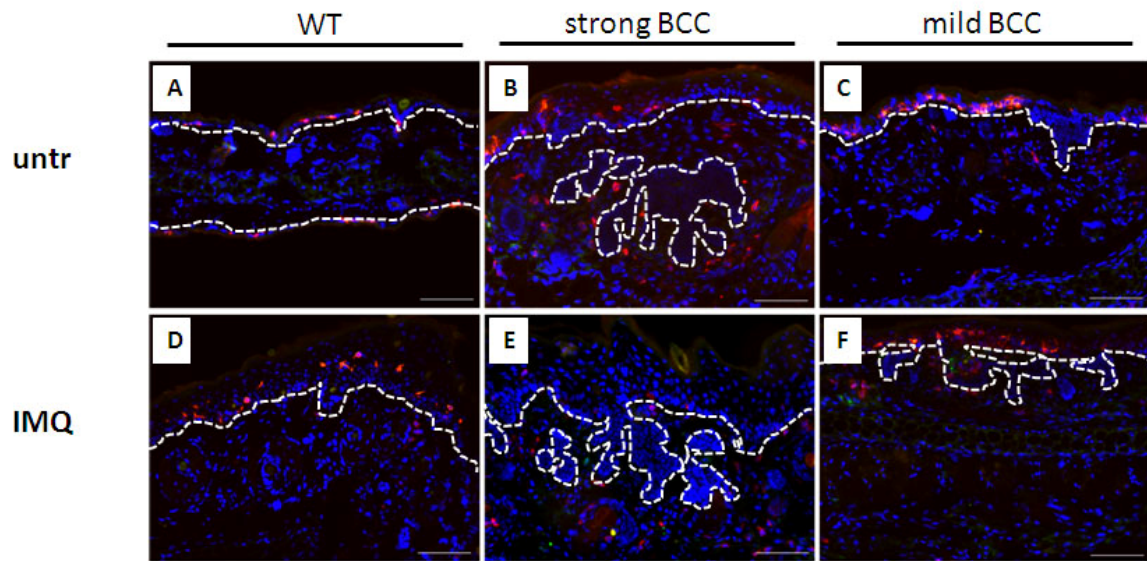
Figure 28: Distribution of γδ T cells in BCC affected skin is altered: Immunofluorescence stainings on cryosections from healthy and BCC bearing mice treated and untreated with Imiquimod; A: untreated healthy mouse, B: untreated BCC showing a strong phenotype, C: untreated BCC showing a mild phenotype, D: Imiquimod treated healthy mouse ear, E: Imiquimod treated BCC showing a strong phenotype, F: Imiquimod treated BCC showing a mild phenotype; G: quantification of γδ T cell numbers in epidermis overlaying BCC of strong and mild phenotype. n = 2-3 mice per group. scale = 100μm
Green: Vγ3; Red: CD3ε; Blue - Hoechst

4. Discussion

Since skin cancers appear with a high incidence (Rogers 2010), it is of importance to study the mechanisms underlying their development and progression. Therefore, many different mouse model systems have been established to examine the impact of a diversity of factors on skin cancer formation (Zaidi 2008). In contrast to BCC, melanoma is a highly aggressive type of skin cancer and often leads to death of patients. During the last decades, different mechanisms of induction of these cancers could be unraveled, resulting in better therapies for patients. One therapeutic agent commonly used for control and clearance of skin tumor growth is the small immune response modifier Imiquimod, which acts as a TLR7 agonist to activate immune cells, resulting in tumor regression especially in BCC patients. Human data suggest that Imiquimod, when topically applied to the skin, activates LCs. Therefore this study tries to evaluate whether the activation of LCs is crucial for the therapeutic effect of Imiquimod.

In my study, two different mouse model systems were chosen to answer this question: (1) the B16F10 melanoma model in *LangerinDTR:EGFP* mice, and (2) the *SmoM2:YFP K5Cre^ERT LangerinDTR:EGFP* mice developing BCC. *LangerinDTR:EGFP* can be efficiently depleted of LCs from the epidermis, thereby monitoring cancer growth in mouse skin lacking LCs.

LC presence does not influence tumor growth of B16F10 melanoma cells in *LangerinDTR:EGFP* mice. Mice depleted of LCs exhibit the same tumor growth rates as WT mice do, suggesting that the tumor progression is independent of the presence of LCs. Aldara-treatment of B16 melanoma of WT and LC-depleted mice results in reduced tumor growth rates in both animal groups compared to untreated control groups. This outcome leads to the conclusion that LCs are not required to mediate the anti-tumoral effects of Imiquimod.

Since it is commonly accepted that immunosuppression in the skin, e.g. mediated by UV irradiation, is associated with a higher risk for skin cancer development, the role of LCs in the B16 melanoma model needs to be evaluated under additional conditions: LC depletion needs to be performed prior to the subcutaneous injection of B16 melanoma cells and sustained until the end of the experiment. This experiment gives answer to two questions: (1) do B16 tumors form earlier in LC depleted mice,

and (2) does Aldara still exhibit its antitumoral effect in mice which have been depleted of LCs prior to melanoma formation?

Although absence of LCs resulted in minor infiltration of tumors by pDC-like MHC-II CD4 DP cells, CD4$^+$ and CD8$^+$ cells after Aldara treatment, tumors in LC depleted mice still respond to Imiquimod treatment. Therefore it can be concluded that under the given conditions, pDC-like cells, as well as CD4$^+$ and CD8$^+$ cells, are at least not alone responsible for mediating the Imiquimod effect.

Analysis of mast cells revealed an increase in total mast cell numbers in both Imiquimod treated WT and LC-depleted mice. Since mast cells are known to be activated by treatment with Aldara cream (Schild 2007), an increase in degranulated mast cells can be observed after Imiquimod application to tumor overlaying skin. A significant difference in the amount of activated mast cells can only be observed between untreated LC-depleted mice and Aldara creamed LC-depleted mice, indicating that the presence of LCs seems to dampen the process of mast cell degranulation.

Since the *LangerinDTR:EGFP* mice harbor the sequence for the DTR under control of the murine Langerin promoter, not only LCs are efficiently depleted of the skin, but also Langerin expressing dDCs. To exactly evaluate the role of LCs in this model system, a mouse model needs to be found, which depletes only LCs from the skin compartment, and not additional Langerin$^+$ dDCs as well. One such model would be the generation of bone-marrow chimeric mice containing WT bone marrow in *LangerinDTR:EGFP* mice.

The development of *SmoM2:YFP* mice (McMahon 2002) gave the opportunity to study the role of the Hedgehog pathway in different cancer types: BCC, rhabdomyosarcoma, and medulloblastoma (Epstein 2008). This pathway is often affected in human BCC patients (~90%) and therefore a major component in control of tumor formation and progression. To establish a BCC mouse system, *SmoM2:YFP* mice were crossed to *K5-Cre^{ERT}* mice and furthermore to *LangerinDTR:EGFP* mice, giving the possibility for inducible activation of the SmoM2 transgene and to also deplete LCs at later timepoints.

In this model the treatment with Imiquimod was adjusted to human treatment conditions. *SmoM2LangerinDTR* mice were treated with Aldara for 5 consecutive days followed by 2 days of recovery. This treatment schedule was followed for 2 weeks – which resembles the treatment duration in the B16F10 melanoma model –

to evaluate the efficiency of Imiquimod application in a mouse BCC model. Unlike in B16F10 tumor bearing mice, histological analysis did not show reduced growth of BCC formations in *SmoM2LangerinDTR* mice after 2 weeks of Aldara application. Human data show that by 2-3 weeks of treatment, Aldara application is accompanied by strong inflammation (swelling, redness, encrustation). 4-6 weeks after starting treatment with Aldara, a regression of the BCC can be observed. Immune cell infiltration into the dermal compartment of *SmoM2LangerinDTR* mice following Imiquimod treatment was observed, showing that Imiquimod exhibits its proinflammatory effects also in *SmoM2LangerinDTR* mice bearing BCC. This is manifested by epidermal thickening upon Imiquimod application and immune cell infiltration into the dermis. Since histological analysis of BCC bearing *SmoM2LangerinDTR* mice showed that a 2 week treatment is not sufficient to clear BCC lesions, Imiquimod treatment will therefore be prolonged to a time span of 6 weeks in ongoing experiments.

I found that in *SmoM2LangerinDTR* mice BCC occurrence is always accompanied by strong melanocyte accumulation around BCC foci, as can be seen in H&E histological stainings. This goes along with human BCC, which is in 85% of the cases accompanied by pigmentation (Altamura, 2009). As Giemsa stainings show, mast cell numbers are also increased in BCC affected mouse skin. Total mast cell numbers are significantly raised after 2 weeks of BCC progression in untreated mice, whereas upon Imiquimod application no furthermore increase in mast cell numbers can be detected. In contrast, the B16F10 melanoma model could show that mast cell degranulation is significantly enhanced in all Imiquimod treated mice.

To observe, which role LCs play in BCC growth and whether LCs do have an inhibitory effect on mast cell degranulation upon Aldara treatment in the BCC model, LC depletion experiments need to be performed with *SmoM2LangerinDTR* mice.

5. Material

5.1 Buffers

Tail DNA preparation – lysis buffer: 50mM TrisHCl pH 8.0, 100mM EDTA, 100mM NaCl, 1% SDS, 0.5mg/ml Proteinase K

Tail DNA preparation – dissolving buffer: 10mM TrisHCl pH 8.0, 1mM EDTA

Epidermal single cell suspension - Würzburg buffer: 1% FCS, 5mM EDTA, 20µg/ml DNaseI

Red blood cell lysis - ACK lysis buffer: 8.024mg/L NH_4Cl, 1.001mg/L $KHCO_3$, 3.722mg/L EDTA

5.2 Reagents and solutions

DPBS - # H15-002; PAA Laboratories

HBSS - # 14175-053; Gibco Invitrogen

FCS - # A15-043; PAA Laboratories

DMEM - # E15-810; PAA Laboratories

Pen/Strep - # P11-010; PAA Laboratories

L-Glutamin 200mM - # M11004: PAA Laboratories

Sodiumbicarbonate - # 1.06329.0500; Merck

Trypsin - # 27250-018; Invitrogen

Gelatine from porcrine skin, Type A - # G1890-100G; Sigma Aldrich

DMSO - # 1.09678.0100; Merck

Perm Wash - # 554723; BD Biosciences

Tamoxifen – # M77181863; Molecula

Sunflower seed oil - # S5007-250; Sigma Aldrich

Ethanol - # 1.00983.2500; Merck

Aldara - # EU/1/98/080/001; Meda AB

DT - # 150; List

Liberase - # 05 401 127 001; Roche

DNaseI - # DN25; Sigma Aldrich

EDTA - # 8418.1000; Merck

Isopropanol - # 1.09634.1011; Merck

TrisHCl - # 4855.2; Roth

SDS - # 4360.2; Roth

Proteinase K - # 03115879001; Roche

Taq-Polymerase - # 11 435 094 001; Roche

Cell culture grade water - # S15-012 PAA Laboratories

dNTPs - # U1240; Promega

10x PCR Buffer - # 11 473 100; Roche

Agarose - # A9539-500G; Sigma Aldrich

Paraformaldehyde - # 8.18715.1000; Merck

OCT Tissue Tek - # 4583; Sakura Finetek Europe

BSA - # A3059-100G; Sigma Aldrich

Normal goat serum – # ; DAKO

Ammoniumthiocyanate - # 1.01213.0500; Merck

Acetone - # 1.00014.1011; Merck

FluoPrep - # 75521; BioMerieux Sa

Entellan - # 1.07961.0100; Merck

Hematoxylin - # HHS32-1L; Sigma Aldrich

Eosin - # HT110132-1L; Sigma Aldrich

Giemsa - # 1.09204.0500; Merck

Acetic acid - # 1.00063.2500; Merck

NeoClear (Xylol-Substitute) - # 1.09843.5000; Merck

Paraffin

ImmEdge Pen - # HH-400; Vector Laboratories

Hoechst 33342 - #B2261-1G; Sigma Aldrich

7'AAD - # 129935; CalBiochem

Needles – Microlance 3 (# 300700; # 300400; # 300300); BD

Syringes – # BS-01T; Terumo Europe

Ketanest - # 400002935; Pfizer

Rompun - # 79055935; Bayer Health Care

NaCl - # 1.06404.1000; Merck

NH_4Cl - # 1.101145.1000; Merck

$KHCO_3$ - # 1.04854.1000; Merck

$MgCl_2$ - # 2189.1; Roth

$(NH_4)_2SO_4$ - # 1.01216.1000 Merck

5.3 Antibodies

CD3e – A488 - # 100321; BioLegend

CD3e – PE - # 553064; BD Pharmingen

CD4 – FITC - # 553729; BD Pharmingen

CD4 – PE - # 553653; BD Pharmingen

CD3e – PE-Cy7 - # 100320; BioLegend

CD8a – FITC - # 553031; BD Pharmingen

CD8a – Horizon - # 560469; BD Pharmingen

CD11b – Pb - # 101224; BioLegend

CD11c – FITC - # 553801; BD Pharmingen

CD11c – APC - # 550261; BD Pharmingen

CD45 – APC-Cy7 - # 103116; BioLegend

CD45R (B220) – APC - # 553092; BD Pharmingen

CD103 – PE - # 121406; BioLegend

CD115 – PE - # 135506; BioLegend

CD207 (Langerin) – FITC - # DDX0362; Dendritics

CD326 (EpCAM) – FITC - # 118210; BioLegend

F4/80 – Pe-Cy7 - # 123114; BioLegend

GR-1 – PE - # 553108; BD Pharmingen

Ly6C – APC - # 560595; BD Pharmingen

MHC-II – FITC - # 553623; BD Pharmingen

MHC-II – PE - # 107608; BioLegend

MHC-II – Pb - # 107620; BioLegend

mPDCA-1 – FITC - # 120-002-289; MACS Miltenyi Biotec

NK1.1 – APC - # 17-5941-81; eBioscience

Vg3 – FITC - # 553229; BD Pharmingen

CD16/32 - # 101302; BioLegend

Active caspase-3 - # 557035; BD Pharmingen

Phospho-Ser10-HistoneH3 - #9701 ; Cell Signaling

anti-rabbit-A488 - # A11034; Invitrogen

anti-rabbit-A594 - # A11012; Invitrogen

anti-rat-A488 - # A11006; Invitrogen

anti-rat-A594 - # A11007; Invitrogen

5.4 Primer

<u>Langerin-DTR:</u>

LangEGFP forward – 5'GAA TGA CAG ATC TGG CCT GAG CTC G –3'

LangEGFP reverse – 5'GTA GCT TTT ATA TGG TCA GCC AAG G –3'

<u>SmoM2:</u>

HE1 (detects YFP) forward – 5'CTG ACC CTG AAG TTC ATC TGC –3'

HE2 (detects YFP) reverse – 5'GTG CGC TCC TGG ACG TAG – 3'

WT3621 – 5'CGT GAT CTG CAA CTC CAG TC –3'

WT316 – 5'GGA GCG GGA GAA ATG GAT ATG –3'

5.5 Mice

Langerin-DTR:EGFP mice were a kind gift from Prof. Dr. Adrien Kissenpfennig. They were maintained in C57BL/6 background. Via injection of DT, these mice efficiently get depleted of LCs and Langerin[+] dDCs 24h after injection.

Prof. Dr. Fritz Aberger kindly provided *Rosa26SmoM2YFP* mice, which were backcrossed to *K5-Cre[ERT]* C57BL/6 mice, to allow tamoxifen inducible activation of the smoothened transgene in the skin. Furthermore, *Rosa26SmoM2YFP K5Cre[ERT]* were crossed to *LangerinDTR:EGFP* mice to generate BCC developing mice that can be depleted of LCs.

5.6 Equipment

Epifluorescence and Light Microscope – Nikon Eclipse 80i

Confocal Fluorescence Microscope - Zeiss

FACS – BD LSR-II

Schiebelehre

5.7 Software

Epifluorescence and Light Microscope – Nikon LuciaG

FACS - BD FACSDiva Software for recording

FACS – FlowJo for analysis

6. Methods

6.1 Animal handling and tissue preparation

All animal experiments were approved the Ethics Committee of the Medical University of Vienna. All mice were treated according to institutional guidelines.

6.1.1 Tumor models

6.1.1.2 B16F10 melanoma growth protocol

6.1.1.2.1 Cell culture and melanoma cell injection

B16F10 melanoma cells were cultured in DMEM supplemented with 10% FCS, penicillin/streptomycin, glutamate and sodiumbicarbonate for 2 – 3 passages at 37°C. During each passage they were washed twice with 1x PBS, trypsinized for 1 min, washed twice with medium and split into 0.1% gelatine coated cell culture flasks. For injection into mice, cells were grown until they reached 60-70% confluence, washed twice with 1x PBS, trypsinized for 1 min, washed twice with PBS and finally diluted to a concentration of $7 \cdot 10^5$ $^{cells}/_{ml}$ with 1x PBS. Cells were kept on ice until injected $3.5 \cdot 10^4$ $^{cells}/_{mouse}$ subcutaneously into anesthesized Langerin-DTR:EGFP mice.

6.1.1.2.2 B16F10 melanoma growth monitoring and treatment

Tumors appeared 7-10 days after subcutaneous injection and were measured in diameter from two sides (A and B) using a mechanical caliper rule. Tumor volume was calculated from the excel formula

=MAX(Rohdaten!A:B)*MIN(Rohdaten!A:B)^2*PI()/6

Tumors were measured every second day and growth was monitored until tumor size was ethically inconsistent. Mice were then sacrificed and parts of the tumor were embedded into OCT tissue tek, fixed in 4% paraformaldehyde for further paraffin embedding, and FACS analyzed (see 6.1.6).

Tumor bearing *Langerin-DTR:EGFP* were subdivided into four groups: untreated, LC-depleted, Imiquimod-treated and LC-depleted Imiquimod treated. Aldara was applied topically to tumor-overlaying skin as well as to tumor-proximate skin. All Imiquimod treated mice were separated from non-Imiquimod treated mice to avoid systemic side effects among treated and untreated groups by licking the treated area. Imiquimod application occurred every second day along with tumor size measurement. LC-depletion of mice was performed via injection of diphtheria toxin i.p. in a concentration of 200ng/mouse every fourth day to ensure consistent depletion of LCs during the whole experimental time duration.

6.1.1.3 BCC induction and treatment protocol

Rosa26SmoM2YFP (K5Cre^ERT) Langerin-DTR:EGFP mice were given 30µl of tamoxifen (10 mg/ml) daily from P10 – P15, followed by tamoxifen injections once a week (concentration depending on weight of mice) until they got sacrificed. By P60-P80, first BCC lesions were observed. At day 90 mice were subdivided into four groups: WT untreated, WT Imiquimod treated, BCC untreated and BCC Imiquimod treated mice. At the first day of treatment (day 0), mice were anesthesized and one ear was cut off, to be used for frozen and paraffin histology as well as for preparation of epidermal ear sheets. Aldara was applied topically on the residing ear and the tail. Imiquimod treatment occurred twice for 5 consecutive days, separated by 2 days of recovery. At day 102 (experimental day 12), mice were sacrificed and ear, back and tail skin were frozen in OCT tissue tek, fixed in 4% paraformaldehyde and processed for FACS analysis (see 6.1.5).

6.1.2 Tail DNA preparation

5mm of tail tip were cut off with an ethanol cleaned scissor and added to 500µl of tail buffer. Prior to use, tail buffer was supplemented with 0.5mg/ml Proteinase K. Tail tubes were incubated over night at 55°C to allow tissue digestion. 200 µl of 6M NaCl

were added and tubes were centrifuged for 10 min at 13,000 rpm. Supernatants were transferred to a fresh tube and 500 µl of isopropanol were added. After centrifugation for 10 min at 13,000 rpm, supernatant was removed and pellet was washed with 70% ethanol. Pellets were air-dried after centrifugation for 15 min at 13,000 rpm and dissolved in 500 µl of TE buffer, shaking 2-3 h at 37°C. Tail tubes were stored at 4°C.

6.1.3 Anesthesia

Ketanest   10 ml

Rompun   2 ml

Aqua dest.   28 ml

6.1.4 Melanoma cell injection

B16F10 melanoma cells were suspended in 1x PBS and kept on ice until injected intradermally at a concentration of $3.5 \cdot 10^4$ $^{cells}/_{mouse}$ into anesthesized *Langerin-DTR:EGFP* mice.

6.1.5 Preparation of epidermal ear sheets

Ears were cut off and dorsal half was separated from ventral half. Then they were collected dermal-side down on 1x PBS and kept on 4°C over night or processed immediately. Ears were transferred onto 0.1% ammoniumthiocyanate solution and incubated for 25 min at 37°C. Thereafter, epidermis was peeled off with forceps and washed three times with 1x PBS for 5 min each. Epidermal sheets were then fixed in 4% paraformaldehyde for 30 min at 4°C, washed three times with 1x PBS for 5 min each and finally frozen in 2% BSA in PBS.

6.1.6 Skin single cell suspension

Ears and tail were cut off from mice; ears got separated into dorsal and ventral half, whereas tail skin was freed from vertebral bodies. Skin parts were cut into small pieces (5-10 mm^2) and collected in a 50ml Falcon tube containing 2ml of HBSS supplemented with 0.15 mg/ml liberase & 0.12 mg/ml DNaseI. Tubes were incubated

in the water bath for 1h at 37°C. Afterwards 0,01 mM EDTA were added to stop the digestion reaction and skin fragments were pipetted up and down extensively in additional 5 ml of Würzburg buffer. The obtained cell suspension was added on a Falcon cell strainer positioned on a fresh tube. Another 5ml of Würzburg buffer were pipetted onto the cell strainer to increase the cell yield. Cells were centrifuged for 5 min at 1,260 rpm at 16°C and washed in PBS-FCS (1x PBS containing 8% FCS). Cells were counted at the CASY cell counter and resuspended in appropriate volumes of PBS-FCS to achieve final concentrations of $1 \cdot 10^6$ cells/FACS staining.

6.1.7 Tumor single cell suspension

B16F10 melanomas were isolated from *LangerinDTR:EGFP* mice and freed from tumor-overlaying skin. Tumors were cut into small pieces and collected in 2ml eppendorf tubes containing 1,2 ml of PBS supplemented with liberase [10 µg/ml]. Tubes were incubated in a thermo shaker, shaking at 900 rpm for 1h at 37°C. The solution was homogenized by pipetting up and down and transferred to a cell strainer positioned on a 50ml falcon tube. 10 ml of PBS-FCS were added onto the cell strainer to increase the cell yield and to stop the digest. Cells were centrifuged for 5 min at 1,260 rpm at 16°C and dissolved in 3ml of ACK lysis buffer to remove red blood cells. Immediately after homogenization, 3 ml of PBS-FCS were added to stop the reaction. Cells were centrifuged for 10 min at 1,260 rpm at 16°C and washed in PBS-FCS. After centrifugation for 5 min at 1,260 rpm at 16°C, cells were counted on a CASY cell counter and resuspended in appropriate volumes of PBS-FCS to achieve final concentrations of $1 \cdot 10^6$ cells/FACS staining.

6.2. Immunology

6.2.1 FACS analysis

6.2.1.1 Extracellular staining of cells

Single cell suspensions from whole-skin and B16F10 tumors were transferred to Micronic FACS tubes and incubated with Fc-Block for 5 min on ice. 5µl of each antibody mixture for extracellular molecules were propounded into the staining FACS tubes and 50µl of each cell suspension were added (note: not only whole antibody mixtures were used, but also single staining of every stained color occurred for proper emission compensation during the FACS recording). After vortexing, cells were incubated for 25 min in the dark on 4°C. Cells were washed twice with 500 µl PBS-FCS, centrifuged for 5 min at 1,260 rpm at 16 °C, and vortexed after every washing step. For analysis, they were diluted in a volume of 50µl.

6.2.1.2 Intracellular staining of cells

After extracellular staining of cells, the cells were fixed in 200 µl 2% paraformaldehyde at least for 30 min. Afterwards, they were washed twice in 500 µl PBS-FCS, then washed twice in 500 µl perm wash, followed by incubation in 100 µl perm wash for 15 min. Cells were then washed once more in 500 µl perm wash. 5 µl of antibody mixture for intracellular antibodies were added, the whole mix got vortexed and incubated for 25 min at 4°C in the dark. After another two washing steps with 500µl PBS-FCS, cells were diluted in a final volume of 50 µl.

6.3. Microscopy

6.3.1. Immunofluorescence

6.3.1.1 Cryosections

5µm tissue sections were performed in a diameter of   at a HM500OM Microm Cryostat. Until further use, tissue samples were stored at -80°C, whilst frozen sections were stored at -20°C. For immunofluorescent stainings, cryosections were temperature equilibrated and air-dried for 10 min at room temperature. Following fixation in ice cold acetone for 20 min, samples were air-dried again for 10 min and then washed in 1x PBS trice for 5 min each. The area around the sections was dried carefully with a paper towel and a circle was drawn around every section with a TAP-Pen. Slides were positioned in a humid chamber and each section was incubated in 100µl blocking solution (10% goat serum in 2% BSA-PBS) for 30 min at room temperature. After removing the blocking solution, 100 µl of antibody mixtures (antibodies diluted in 2% BSA-PBS) were pipetted onto each section and the slides were incubated at 4°C over night. Afterwards, sections were washed three times 5 min each in 1x PBS and then incubated in 100 µl 1 mg/ml Hoechst for 20 min. After washing 3 times for 5 min each in 1x PBS, sections were mounted in FluoPrep aquaeous mounting medium and stored in the dark at 4°C until further usage for microscopy.

6.3.1.2. Ear sheets

After preparation of epidermal ear sheets (see 6.1.4 Epidermis-dermis separation), a part of every frozen epidermal sheet was cut off with a scalpel knife and transferred into a chamber of a 48 well plate, each chamber filled with 100 µl blocking solution (10% goat serum in 2% BSA-PBS). After incubation for 30 min at room temperature, blocking solution was removed with a pipette and 100µl of antibody mixture (antibodies diluted in 2% BSA-PBS) were added. Incubation occurred at 4°C in the dark over night. Sheets were then washed for three times 5 min each and incubated for 20 min with 100 µl Hoechst at room temperature. After washing twice for 5 min

each, sheets were transferred to glass slides and spread with forceps under a binocular light microscope. Finally, ear sheets were mounted in FluoPrep and kept at 4°C in the dark until further use for microscopy.

6.3.2. Light microscopy

6.3.2.1. H&E

Paraffin embedded tissue samples were cut in a diameter of 5 µm at a microtome and applied to DAKO microcapillar 70µm glass slides. They were stored at room temperature until usage for histological staining. After minimum 30 min incubation of glass slides at 55°C, the sections were deparaffinized in NeoClear for 2x 1 min, followed by rehydration: 2x 100% ethanol, 2x 70% ethanol, 2x distilled water for 1 min each. Slides were incubated in freshly filtrated Hematoxylin for 5 min and differentiated in flowing tap water for 5 min and incubation in HCl-water for 5 sec. After incubation in distilled water for 1 min, slides were incubated in Eosin for 45 sec, followed by a dehydration series: 2x 96% ethanol, 2x 100% ethanol, 2x NeoClear for 1 min each. Sections were mounted in the non-aquaeous mounting medium Entellan and stored at room temperature until further use.

6.3.2.2. Giemsa

Paraffin embedded tissue samples were cut in a diameter of 5 µm at a microtome and applied to DAKO microcapillar 70µm glass slides. They were stored at room temperature until usage for histological staining. After minimum 30 min incubation of glass slides at 55°C, the sections were deparaffinized in NeoClear for 2x 1 min, followed by rehydration: 2x 100% ethanol, 2x 70% ethanol, 2x distilled water for 1 min each. Sections were incubated in freshly prepared Giemsa solution (Giemsa stock solution diluted 1:3 in distilled water) for 18 min. For differentiation, sections were first transferred to 0.1% acetic acid for 2 min and then incubated in 96% ethanol for 1 min. After dehydration in 2x 96% ethanol, 2x 100% ethanol and 2x NeoClear for 1 min each, sections were mounted in the non-aquaeous mounting medium Entellan and stored at room temperature until further use.

6.4 Statistical analysis

Mice from *Langerin-DTR:EGFP* B160F10 melanoma model were grouped into untreated, LC-depleted, Imiquimod treated and LC-depleted Imiquimod treated mice, whereas *Rosa26SmoM2YFP K5Cre^{ERT} Langerin-DTR:EGFP* mice were grouped into WT untreated, WT Imiquimod treated, BCC untreated and BCC Imiquimod treated mice. Variance of LC density, mast cell frequency, epidermal thickness, and immune cell infiltration into B16 melanoma tumors, BCC lesions and skin within the groups was measured. Statistical analysis was performed using the two-sided Student´s t-test.

$p < 0,05$ (*)

$p < 0,01$ (**)

$p < 0,001$ (***)

7. References

Ackermann J, Frutschi M, Kaloulis K, McKee T, Trumpp A, Beermann F (2005) Metastasizing melanoma formation caused by expression of activated N-RasQ16K on an INK4a-deficient background, Cancer Res 65, 4005-4011.

Altamura D, Menzies SW, Argenziano G, Zalaudek I, Soyer HP, Sera F, Avramidis M, DeAmbrosis K, Fargnoli MC, Peris K (2009) dermatoscopy of basal cell carcinoma: morphologic variability of global and local features and accuracy of diagnosis, J Am Acad Dermatol

Asselin-Paturel C and Trinchieri G (2005) Production of type I interferons: pDCs and beyond, J Exp Med 202, 461-465.

Barchet W, Cella M, Colonna M (2005) pDCs – virus experts of innate immunity, Semin Immunol 17, 253-261.

Bergers G and Benjamin LE (2003) Tumorigenesis and the angiogenic switch, Nat Rev Cancer. 3, 401-10.

Berking, Takemoto R, Satyamoorthy K, Shirakawa T, Eskandarpour M, Hansson J (2004) Induction of melanoma phenotypes in human skin by growth factors and UVB, Cancer Res 64, 807-811.

Birbeck MD, Breathnach AS, Everall JD (1961) An electron microscopy study of basal melanocytes and high-level clear cells (LCs) in vitilgo, J Invest Dermatol 37, 51.

Boismenu R, Havran WL (1998) gd T cells in host defense and epithelial cell biology. Clin Immunol Immunopathol 86, 121-133

Bosenberg MW (2003) Skin cancer models, National cancer institute – mouse models of human cancers consortium , http://emicestage.nci.nih.gov/mouse_models/organ_models/skin_models.

Borkowski TA, LEtterio JJ, Farr AG, Udey MC (1996) A role for endogenous TGFb1 in LC biology: the skin of TGFb1 null mice is devoid of epidermal LCs, J Exp Med 184, 2417-2422.

Cao W and Liu YJ (2007) Innate immune functions of plasmacytoid dendritic cells, Curr Opin Immunol 19, 24-30.

Cao W, Bover L, Cho M, Wen X, Hanabuchi S, Bao M, Rosen D, Wand YH, Shaw JL, Du Q, Li C, Arai N, Yao Z, Lanier LL, Liu YJ (2009) Regulation of TLR7/9 responses in pDCs by BST2 and ILT7 interaction, J Exp Med 206, 1603-1614.

Chin L, Garraway LA, Fisher DE (2006) Malignant melanoma: genetics and therapeutics in the genomic era, Genes Dev 20, 2149-4182.

Cisse B, Caton ML, Lehner M, Maeda T, Scheu S, Locksley R, Holmberg D, Zweier C, den Hollaner NS, Kant SG, Holter W, Rauch A, Zhuang Y, Reizis B (2008) Transcription Factor E2-2 is an essential and specific regulator of pDC development, Cell 135, 37-48

Clark RA, Huang SJ, Murphy GF, Mollet IG, Hijnen D, Muthukuru M, Schanbacher CF, Edwards V, Miller DM, Kim JE, Lambert J, Kupper TS (2008) Human squamous cell carcinomas evade the immune response by down-regulation of vascular E-selectin and recruitment of regulatory T cells, J Exp Med 205, 2221-2234

Colonna M, Trinchieri G, Liu YJ (2004) pDCs in immunity, Nature Immunol 5, 1219-1226.

Corcoran RB, Scott MP (2001) A mouse model for medulloblastoma and basal cell nevus syndrome, J Neurooncol 53, 307-318.

De Giorgi V, Salvini C, Chiarugi A, Paglierami M, Maio V, Nicoletti P, Santucci M, Carli P, Massi D (2009) *In vivo* characterization of the inflammatory infiltrate and apoptotic status in Imiquimod-treated basal-cell carcinoma, Int J Dermatol 48, 312-321.

Diebold SS, Kaisho T, Hemmi H, Akira S, Reis e Sousa C (2001) Innate antiviral responses by means of TLR7-mediated recognition of ssRNA, Science 303, 1529-1531.

Eckert RL (1989) – Structure, function, and differentiation of the keratinocyte, Physiol Rev 69, 1316-1346.

Epstein EH (2008) Basal cell carcinomas: attack of the hedgehog, Nat Rev Cancer 8, 743-754.

Ferrara N, Gerber HP, and LeCouter J (2003) The biology of VEGF and its receptors, Nat Med 9, 669–676.

Fidler IJ and Kripke ML (1977) Metastasis results from preexisting variant cells within a malignant tumor, Science 197, 893-895.

Freedberg IM, Tomic-Canic M, Komine M, Blumenberg M (2001) Keratins and the keratinocyte activation cycle, J Invest Dermatol 116, 633-640.

Gailani MR et al (1992) Developmental defects in Gorlin syndrome related to a putative tumor suppressor gene on chromosome 9, Cell 69, 111-117.

Gailani MR et al (1996) The role of the human homologue of *Drosophila* patched in sporadic basal cell carcinomas, Nature Genet 14, 78-81.

Gaitanis G, Nomikos K, Vava E, Alexopoulos EC, Bassukas ID (2009) Immunocryosurgery for basal cell carcinoma: results of a pilot, prospective, open-label study of cryosurgery during continued Imiquimod application, Europ Acad Dermatol Ven

Gilliam AC et al (1998) The human hair follicle: a reservoir of CD40+ B7-deficient Langerhans cells that repopulate epidermis after UVB exposure, J Invest Dermatol 110, 422-427.

Gilliet M, Cao W, Liu YJ (2008) pDCs: sensing nucleic acids in viral infection and autoimmune diseases, Nat Rev Immunol 8, 594-606.

Granstein RD, Matsui MS (2004) UV-radiation induced immunosuppression and skin cancer, Cutis 74, 4-9.

Gray-Schoper VC, Cheong SC, Chong H, Chow J, Moss T, Abdel-Malek ZA et al (2006) Cellular senescence in naevi and immortalization in melanoma: a role for p16?, Br J Cancer 95, 496-505.

Gupta GP, Minn AJ, Kang Y, Siegel PM, Serganoca I, Cordon-Cardo C (2005) Identifying site-specific metastasis genes and functions, Cold Spring Harb Symp Quant Biol 70, 149-158.

Hahn H, Wojnowski L, Miller G, Zimmer A (1999) The patched signaling pathway in tumorigenesis and development: lessons from animal models, J Mol Med 77, 459-468.

Hart IR and Fidler IJ (1980) Role of organ selectivity in the determination of metastatic patterns of B16 melanoma, Cancer Res 40, 2281-2287.

Heib V, Becker M, Warger T, Rechtsteiner G, Tertilt C, Klein M, Bopp T, Taube C, Schild H, Schmitt E, Stassen M (2007) Mast cells are crucial for early inflammation, migration of LCs and CTL responses following topical application of TLR7 ligand mice, Blood 110, 946-953.

Heil F et al (2004) Species-specific recognition of ssRNA via TLR7 and 8, Science 303, 1526-1529.

Hemmi H et al (2000) TLR recognizes bacterial DNA, Nat Rev Immunol 408, 740-745.

Hemmi H et al (2001) Skin antigens in the steady state are trafficked to regional LNs by TGFb dependent cells, Int Immunol 13, 695-704.

Hemmi H, Kaisho T, Takeuchi O, Sato S, Sanjo H, Hoshino K, Horiuchi T, Tomizawa H, Takeda K, Akira S (2002) Small anti-viral compounds activate immune cells via the TLR MyD88-dependent signaling pathway, Nat Immunol 3, 196.

Holt PG, Haining S, Nelson DJ, Sedgwick JD (1994) Origin and steady-state turnover of class II MHC-bearing dendritic cells in the epithelium of the conducting airways, J Immunol 153, 256-261.

Huang SJ, Hijnen D, Murphy GF, Kupper TS, Calarese AW, Mollet IG, Schanbacher CF, Miller DM, Schmults CD, Clark RA (2009) Imiquimod enhances IFNg production and effector function of T cells infiltrating human squamous cell carcinomas of the skin, J Invest Detmatol 129, 2676-2685.

Jakob T, Ring J, Udey MC (2001) Multistep navigation of LCs/DCs in and out of the skin, J Allergy Clin Immunol 108, 688-696

Jameson J, Havron WL (2009) A role for human skin-resident T cells in wound healing, J Exp Med 206, 743-750

Jarosay D, Napolitani G, Colonna M, Sallusto F, Lanzavecchia A (2001) Specialization and complementarity in microbial molecule recognition by human myeloid and plasmacytoid DCs, Eur J Immunol 31, 3388-3393.

Jego G et al (2003) pDCs induce plasma cell differentiation through type I interferon and IL-6, Immunity 19, 225-234.

Johnson RL et al (1996) Human homolog of patched, a candidate gene for the basal cell nevus syndrome, Science 272, 1668-1671.

Jurk M et al (2002) Human TLR7 and 8 independently confer responsiveness to the antiviral compound R-848, Nature Immunol 3, 499-499.

Kadowaki N et al (2001) subsets of human DC precursors express different TLRs and respond to different microbial antigens, J Exp Med 194, 863-870.

Kannan K, Sharpless NE, Xu J, O´Hagan RC, Bosenberg M, Chin L (2003) Components of the Rb pathway are critical targets of UV mutagenesis in a murine melanoma model, Proc Natl Acad Sci USA 100, 1221-1225.

Karjalainen K (2000) Anatomical origin of DCs determines their life span in peripheral LNs, J Immunol 165, 4910-4916.

Kissenpfennig A, Henri S, Dubois B, Laplace-Builhé C, Perrin P, Romani N, Tripp CH, Douillard P, Leserman L, Kaiserlian D, Saeland S, Davoust J, Malissen B (2005) Dynamics and function of LCs in vivo: dDCs colonize LN areas distinct from slower migrating LCs, Immunity 22, 643-654

Klechevsky E et al (2008) Functional specializations of human epidermal Langerhans cells and CD14+ dermal dendritic cells, Immunity 29, 497-510.

Klein-Szanto AJ, Silvers WK, Mintz B (1994) UV radiation-induced malignant skin melanoma in melanoma-susceptible transgenic mice, Cancer Res 54, 4569-4572.

Kolumam GA, Thomas S, Thompson LJ, Sprent J, Murali-Krishna K (2005) Type I interferons act directly on CD8 T cells to allow clonal expansion and memory formation in response to viral infection, J Exp Med 202, 637- 650.

Kricker A, Armstrong BK, English DR, Heenan PJ (1995) Does intermittent sun exposure cause basal cell carcinoma? A case-control study in Western Australia, Int J Cancer 60, 489-494.

Laird R, Hayes S (2009) Profiling of the early transcriptional response of murine gd T cells, Mol Immunol

Le Bon A et al (2008) Cross priming of CD8+ T cells stimulated by virus-induced type I interferon, Nature Immunol 4, 1009-1015.

Lichtenberger BM, Tan PK, Niederleithner H, Ferrara N, Petzelbauer P, Sibilia M (2010), Cell 140, 268-79.

Lum L and Beachy PA (2004) The Hedgehog response network: sensors, switches, and routers, Science 304, 1755-1759.

Lund LP and Timmins GS (2007) Melanoma, long wavelength UV and sunscreens: controversies and potential resolutions, Pharmacol Ther 114, 198-207.

Macatonia SE, Knight SC, Edwards AJ, Griffiths S, Fryer P (1987) Localization of antigen on LN DCs after exposure to the contact sensitizer FITC. Functional and morphological study, J Exp Med 166, 1654-1667.

Maddodi N, Setaluri V (2008) Role of UV in cutaneous melanoma, Photochem Photobiol 84, 528-536.

Maldonado-López R et al (1999) CD8a+ and CD8a- subclasses of dendritic cells direct the development of distinct T helper cells *in vivo*, J Exp Med 189, 587-592.

Mao J, Ligon KL, Rakhlin EY, Thayer SP, Bronson RT, Rowitch D, McMahon P (2006) A novel somatic mouse model to survey tumorigenic potential applied to the hedgehog pathway, Cancer Res 66, 10171-10178.

Mardones F, Zemelman V, Sarzunic I, Morales C, Palma K, Vargus M (2009) CD1a+ Langerhans cells in the peritumoral epidermis of basal-cell carcinoma, Actas Dermosfiliogr 100, 700-705.

Mc Dermott R et al (2002) Birbeck granules are subdomains of endosomal recycling compartement in human epidermal LCs, which form where langerin accumulates, Mol Biol Cell 13, 317-335.

Mehling A et al (2001) Overexpression of CD40ligand in murine epidermis results in chronic skin inflammation and systemic autoimmunity, J Exp Med 194, 615-628.

Merad M et al (2002) Langerhans cells renew in the skin throughout life under steady-state conditions, Nature Immunol 3, 1135-1141.

Merad M et al (2004) Depletion of host Langerhans cells before transplantation of donor alloreactive T cells prevents skin graft-versus-host-disease, Nature Med. 10, 510-517.

Merad M, Ginhoux F, Collin M (2008) Origin, homeostasis and function of Langerhans cells and other langerin-expressing DCs, Nat Rev Immunol 8, 935-947

Miller AJ, Mihm MC Jr (2006) Melanoma, N Engl J Med 355, 51-65

Miller RL et al (1999) Imiquimod applied topically: a novel immune response modifier and a new class of drug, Int J Immunopharmacol 21, 1-14.

Mooi WJ, Peeper DS (2006) Oncogene-induced cell senescence – halting on the road to cancer, N Engl J Med 335, 1037-1046.

Moser M, Murphy KM (2002) Dendritic cell development of TH1 – TH2 development, Nat Immunology 1, 199-205.

Naik 2007 – Development of plasmacytoid and conventional DC substypes from single precursor cells

Nakajima C, Ueksa Y, Iwasaki M, Yamaguchi N, Mukai T, Gao P (2001) A role of IFNg in tumor immunity: T cells with the capacity to reject tumor cells are generated but fail to migrate to tumor sites in IFNg-deficient mice, Cancer Res 61, 3399-3405.

Nestle F, Meglio P, Yin JZ, Nickoloff B (2009) Skin immune sentinels in health and disease, Nat Rev Immunol 9, 679-691.

Noonan FP, Recia JA, Takayama H, Duray P, Anver MR, Rush WL (2001) Neonatal sunburn and melanoma in mice, Nature 413, 271-272.

Ohl L et al (2004) CCR7 governs skin DC migration under inflammatory and steady-state conditions, Immunity 21, 279-288.

Palamara F, Meindl S, Holcmann M, Lührs P, Stingl G, Sibilia M (2004) – Identification and characterization of pDC-like cells in normal mouse skin and melanomas treated with Imiquimod, J Immunol, 173, 3051-3061.

Pierre P et al (1997) Developmental regulation of MHC class II transport in mouse DCs, Nature 388, 787-792.

Piqueras B, Connolly J, Freitas H, Palucka AK, Banchereau J (2006) Upon viral exposure, myeloid and plasmacytoid DCs produce 3 waves of distinct chemokines to recruit immune effectors, Blood 107, 2613-2618.

Poulin LF et al (2007) The dermis contains langerin+ DCs that develop and function independently of epidermal LCs, J Exp Med 204, 3119-3131.

Proksch E, Brandner JM, Jensen JM (2008) The skin: an indispensable barrier, Exp Dermatol 17, 1063-1072.

Raulet DH (1989) The structure, function and molecular genetivs of the gd T cells: an important source of IL-17, Curr Opin Immunol 20, 353-357

Reifenberger J et al (2005) Somatic mutations in the PTCH, SMOH, SUFUH and TP53 genes in sporadic basal cell carcinomas, Br J Dermatol 152, 43-51.

Rogers HW, Weinstock MA et al (2010) Incidence estimate of nonmelanoma skin cancer in the United States, 2006, Arch Dermatol 146, 283-287.

Romani N et al (2006) Epidermal LCs – changing views on their function in vivo, Immunol Lett 106, 119-125.

Rubin AI, Chen EH, Ratner D (2002) Basal cell carcinoma, N Eng J Med 353, 2262-2269

Santos I, Mello RJ, Santos IB, Santos RA (2010) Quantitative study of Langerhans cells in basal-cell carcinoma with higher or lower potential of local aggressiveness, An Bras Dermatol 85, 165-171.

Schnidar H, Eberl M, Klingler S, Mangelberger D, Kasper M, Hauser-Kronberger C, Regl G, Kroismayr R, Moriggl R, Sibilia M, Aberger F (2009) EGFR signaling synergizes with Hh/Gli in oncogenic transformation via activation of the MEK/ERK/JUN pathway, Cacer Res 69, 1284-1292.

Schön MP, Wienrich BG, Drewniok C, Bong AB, Eberle J, Geilen CC, Gollnik H, Schön M (2004) Death receptor-independent apoptosis in malignant melanoma induced by the small-molecule immune response modifier Imiquimod, J Invest Dermatol 122, 1266-1276.

Schuler G et al (1993) Murine epidermal LCs as a model to study tissue DCs, Adv Exp Med Biol 329, 243-249

Shklovskaya E, Roediger B, Fazekas de St. Groth B (2008) Epidermal and dermal DCs display differential activation and migratory behavior while sharing the ability to stimulate CD4+ T cell proliferation in vivo, J Immunol 181, 418-430.

Shortman K, Liu YJ (2002) Mouse and human dendritic cell subtypes, Nat Rev Immunol 2, 151-161.

Stingl G, Tamaki K, Katz SI (1980) Origin and function of epidermal LCs, Immunol Rev 53, 149-174.

Stoitzner P et al (2006) LCs cross-present antigen derived from skin, Proc Natl Acad Sci USA 103, 7783-7788.

Stoitzner P et al (2008) Tumor immunotherapy by epicutaneous immunization requires Langerhans cells, J Immunol 180, 1991-1998.

Stoitzner P, Tripp CH, Douillard P, Saeland S, Romani N (2005) Migratory LCs in mouse LNs in steady state and inflammation, J Invest Dermatol 125, 116-125.

Suzuki H, Wang B, Shivji GM, Toto P, Amerio P, Tomai MA, Miller RL, Sauder DN (2000) Imiquimod, a topical immune response modifier, induces migration of LCs, J Invest Dermatol 114, 135.

Tang A, Amagai M, Granger LG, STanles Jr, Udey MC (1993) Adhesion of epidermal LCs to keratinocytes mediated by E-cadherin, Nature 361, 82-85.

Tigelaar RE, Lewis JM, Bergstresser PR (1990) TCRgd+ dendritic epidermal T cells as constituents of skin-associated lymphoid tissue, J Invest Dermatol 94, 51

Tomic-Canic M, Komine M., Freedberg IM, Blumenberg M (1998) Epidermal signal transduction and transcription factor activation in activated keratinocytes, Journal of Dermatological Science 17, 167-181.

Toulon A, Breton L, Taylor KR, Tenenhaus M, Bhavsar D, Lanigan C, Rudolph R, Valladeau J and Saeland S (2005) Cutaneous dendritic cells, Semin Immunol 17, 273-283.

Van den B erg TK, Kraal B (2005) A function for the macrophage F4/80 molecule in tolerance induction, Trends Immunol 26, 506-509.

Valladeau J et al (2000) Langerin, a novel C-type lectin specific to LCs, is an endocytic receptor that induces the formation of Birbeck granules, Immunity 12, 71-81.

Waithman J et al (2007) Skin-derived dendritic cells can mediate deletional tolerance of class I-restricted self-reactive T cells, J Immunol 179, 4535-4541.

Winslow T (2008) http://visualsonline.cancer.gov/details.cfm?imageid=7279

Wolff K (1967) The fine structure of the LC granule, J Cell Biol 35, 468-473.

Xie J et al (1998) Activating Smoothened mutations in sporadic basal cell carcinoma, Nature 391, 90-92.

Xie J et al (2001) A role of PDGFa in basal cell carcinoma proliferation, Proc Natl Acad Sci USA 98, 9255-9259.

Yu Y, Merlino G (2002) Constitutive c-Met signaling through a nonautocrine mechanism promotes metastasis in a transgenic transplantation model, Cancer Res 62, 2951-2956.

Zagon IS, Donahue RN, Rogosnitzky M, McLaughlin PJ (2008) Imiquimod upregulates the opioid growth factor receptor to inhibit cell proliferation independent of immune function, Exp Biol Med 233, 968-979.

http://www.aldara.com/pdfs/aldara_ppi.pdf

8. Appendix

8.1 List of Figures

8.2 List of Abbreviations

7´AAD – 7´actinoaminomycin

A – adenosine

APC – antigen presenting cell

BCC – basal-cell carcinoma

BSA – bovine serum albumin

BTK – bruton´s tyrosine kinase

C – cytosine

CCR – C-C chemokine receptor

CD – cluster of differentiation

CHS – contact-hypersensitivity

CpG – poly-cytosine poly-guanosine

Cre – Cre-recombinase

DC – dendritc cell

dDC – dermal DC

DHH – desert hedgehog

DMEM – Dulbecco´s modified Eagle medium

DMSO – dimethylsulfoxid

DNA – desoxyribonucleic acid

DP – double positive

dNTP – desoxyribonucleosidetriphosphate

DPBS – Dulbecco´s PBS

DT – diphtheria toxin

DTR – diphtheria toxin receptor

EDTA - ethylenediaminetetraacetic acid

EGFP – enhanced green fluorescent protein

EGFR – epithelial growth factor receptor

EpCAM – epithelial cell adhesion molecule

ER – estrogen receptor

ERT – estrogen receptor tamoxifen complex

FACS – fluorescence activated cell sorting

FCS – fetal calf serum

G – guanosine

GEM – genetically engineered mouse

GLI – glioblastoma

H&E – hematoxylin & eosin

HBSS – hank´s buffered salt solution

HCl – hydrochloric acid

Hh – Hedgehog

IFN – interferon

IHH – Indian hedgehog

IL – Interleukin

IMQ – Imiquimod

IRAK – interleukin-1-receptor-associated kinase

K5 – keratin5

LC – Langerhans cell

LN – lymph node

MAPK – mitogen-activated protein kinase

mDC – myeloid DC

MHC – major histocompatibility complex

mPDCA – murine plasmacytoid dendritic cell antigen

MyD88 – myeloid differentiation primary response gene 88

NaCl – sodium chloride

Neo - neomycin

NK – natural killer

OGFR – opioid growth factor receptor

P – postnatal day

PBS – phosphate buffered saline

pDC – plasmacytoid DC

PDGFR – platelet derived growth factor receptor

PI3K – phosphoinositol-3-kinase

PTCH – patched

RGP – radial growth phase

RNA – ribonucleic acid

SCC – squamous cell carcinoma

sDLN – skin draining lymph node

SDS - sodium dodecylsulfate

SHH – sonic hedgehog

SMO – smoothened

SMO DTR-KI/+ - *SmoM2:YFPfl/fl K5CreERT/+ LangerinDTR:EGFP/+*

smoM2 – constitutively active isoform of smo

SP – single positive

ss – single stranded

SUFU – suppressor of fused

T - thymidine

TCR – T cell receptor

TE – Tris-EDTA

TGF – transforming growth factor

T_H1 – T helper 1

TLR – toll-like receptor

TNF – tumor necrosis factor

TRAF – TNF receptor associated factor

UV – ultraviolet

UVR – ultraviolet radiation

VGP – vertical growth phase

WT – wild type

YFP – yellow fluorescent protein

8.3 Curriculum Vitae

Education:

2001-2004   Grimmelshausen-Gymnasium-Gelnhausen, Gelnhausen, Germany

1994-2001   Gymnasium Friedrich-August-Genth-Schule, Wächtersbach, Germany

1991-1994   Elementary school, Jossgrund, Germany

Studies:

2004-2010   Studies of

(1) Molecular biology

(2) Zoology

at the University of Vienna, Austria

Fellowships:

2005-2010   Fellowship of Prof. Dr. Zerweck-/Cassella-Stiftung, Frankfurt am Main, Germany

Employments:

08 2008   Volunteer at Momentum Pharma, Hamburg, Germany

07/08 2006   Organical chemistry laboratory at AllessaChemie, Frankfurt am Main, Germany

07/08 2004   Analytical pharmacy laboratory at AllessaChemie, Frankfurt am Main, Germany

08 2003   Analytical pharmacy laboratory at AllessaChemie, Frankfurt am Main, Germany

Clubs:

Since 2008   Member of Rotaract Wien Innere Stadt, Vienna, Austria

Since 2006   Member of Molecular Biological Society, Vienna, Austria

Since 2002   Member of scuba diving club Bad Orb, Germany